Master's thesis

NTNU
Norwegian University of Science and Technology
Faculty of Engineering
Department of Energy and Process Engineering

Bendik Peter Løvøy Alvestad,
Leon Fevang-Gunn

Effect of Atmospheric Stability on Meandering and Wake Dynamics

Master's thesis in MIENERG and MTPROD
Supervisor: Tania Bracchi
Co-supervisor: Balram Panjwani
June 2023

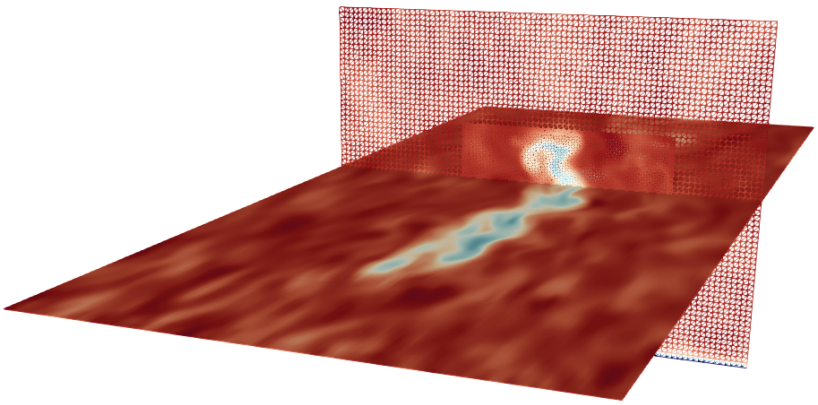

NTNU
Norwegian University of
Science and Technology

Bendik Peter Løvøy Alvestad,
Leon Fevang-Gunn

Effect of Atmospheric Stability on Meandering and Wake Dynamics

Master's thesis in MIENERG and MTPROD
Supervisor: Tania Bracchi
Co-supervisor: Balram Panjwani
June 2023

Norwegian University of Science and Technology
Faculty of Engineering
Department of Energy and Process Engineering

NTNU
Norwegian University of
Science and Technology

Preface

During the spring semester of 2023, we, the authors, conducted and wrote this Master's thesis at the Hydropower Laboratory at the Department of Energy and Process Engineering at the Norwegian University of Science and Technology. The topic of this study is of particular interest to both of us, as we one day aspire to work in the growing offshore wind sector. We are also excited at the prospect of both publishing the paper and potentially taking part in the EERA DeepWind Conference 2024. The thesis is structured as a research article in paper format, aiming to closely resemble a finished publication. The primary document is followed by appendices containing supplementary information that was not included in the research article, but is relevant to the Master's thesis.

Problem description

With the announced increase in energy production from wind farms, understanding the flow dynamics involved allows for more accurate modeling to help with design and optimization. Wake deflection is likely to be viewed as an attractive option within wind farm control. For this technique to mature, however, one of the questions that needs to be addressed further is how the wake behind yawed wind turbines behave in non-neutrally stratified atmospheres, which are dominant offshore, and how well analytical models are able to predict this wake deflection.

This paper intends to investigate the wake dynamics of wind turbines with and without yaw under different atmospheric stabilities. This will be done through large-eddy simulations of the Vestas V80 wind turbine with inflow representing stable, neutral and unstable atmospheres generated using the Mann turbulence generator superimposed onto the wind shear profile. A fast Fourier transform will be performed on the wake meandering, and the energy containing frequencies and wake center position will be studied $8D$ downstream of the wind turbine. Finally, the wake deflection trajectories will be compared with the predictions made by analytical models.

Since these numerical simulations are strictly aerodynamic representations of the wind turbines, the second big question that needs to be addressed for adoption of yaw steering strategies cannot be answered here, namely the structural loads on the wind turbine subject to different wake conditions. Different turbulence generators are not investigated either in the development of this model, and the inflow parameters are based on findings from Riverra-Arreba et al.

Abstract

This study investigates the impact of atmospheric stability on wind turbine flow dynamics, focusing on wake deflection and meandering. High-fidelity numerical simulations using Large-Eddy Simulation with the Actuator Line model are employed to examine three stability conditions for the Vestas V80 turbine with and without yaw. The study is successful in reproducing a numerical representation of the Samsung S7.0-171 turbine, but due to validation data uncertainties, it is not utilized for flow analysis purposes. Results from the study show that meandering occurs around the deflected turbine wake axis. They also indicate that, despite differences in wake deficit and meandering behaviour, neutral and stable cases have similar deflected wake trajectories during yawed turbine operation. The analytical solutions considering wake deflection proposed by other authors show good agreement in the far wake. Spectral analysis of the meandering for neutral and stable cases reveal comparable results for cutoff frequency and peak frequency. Moreover, the calculated Strouhal number is consistent with values found in the literature of $St = 0.16$. The unstable case shows significant differences, but there is some uncertainty associated to these results. Meandering behavior is largely similar between yawed and non-yawed turbines in the unstable and neutral case, while for the stable case slightly larger amplitudes are observed for the yawed condition. More generally, an increase in stability decreases both amplitude and frequency of oscillations.

Sammendrag

Denne studien undersøker effekten av atmosfærisk stabilitet på strømningsdynamikken bak vindturbiner, med fokus på "wake deflection" og "wake meandering". Numeriske Large-Eddy simuleringer med en "Actuator Line" modell blir brukt for å undersøke tre atmosfæriske stabiliteter for Vestas V80-turbinen med og uten yaw. Studien lykkes med å gjenskape en numerisk representasjon av en Samsung S7.0-171-turbin, men grunnet usikkerhet i valideringsdataen, blir den ikke brukt til strømningsanalystiske formål. Resultatene fra studien viser at "meandering" forekommer rundt aksen som følger turbinens wake for turbiner i yaw. De indikerer også at selv om det er forskjeller i "wake deficit" og "wake meandering", følger nøytrale og stabile tilfeller lik "wake-bane" når turbinen er i yaw. Åtte rotordiametere nedstrøms for turbinen finner noen analytiske modeller god overenstemmelse med de numeriske resultatene for "wake-deflection". Spektralanalyse av "meandering" for nøytrale og stabile tilfeller viser sammenlignbare resultater for "cutoff" frekvens og "peak" frekvens. Videre er det beregnede Strouhal-tallet konsistent med verdier funnet i litteraturen for $St = 0.16$. Resultatene for den ustabile atmosfæren, viser betydelige forskjeller fra de andre atmoslæriske forholdene, men det er usikkerhet knyttet til disse resultatene. "Wake meandering" er i hovedsak lik for turbiner med og uten yaw i de ustabile og nøytrale tilfellene. For det stabile tilfellet observeres litt større amplituder for turbiner i yaw. Generelt sett fører økt stabilitet til redusert amplitude og oscilleringsfrekvens.

Effect of Atmospheric Stability on Meandering and Wake Dynamics

Bendik Peter Løvøy Alvestad
Department of Energy and Process Engineering,
NTNU,
Trondheim, Norway
email: bendik.alvestad@gmail.com

Leon Fevang-Gunn[1]
Department of Energy and Process Engineering,
NTNU,
Trondheim, Norway
email: leon.fevanggunn@gmail.com

This study investigates the impact of atmospheric stability on wind turbine flow dynamics, focusing on wake deflection and meandering. High-fidelity numerical simulations using Large-Eddy Simulation with the Actuator Line model are employed to examine three stability conditions for the Vestas V80 turbine with and without yaw. The study is successful in reproducing a numerical representation of the Samsung S7.0-171 turbine, but due to validation data uncertainties, it is not utilized for flow analysis purposes. Results from the study show that meandering occurs around the deflected turbine wake axis. They also indicate that, despite differences in wake deficit and meandering behaviour, neutral and stable cases have similar deflected wake trajectories during yawed turbine operation. The analytical solutions considering wake deflection proposed by other authors show good agreement in the far wake. Spectral analysis of the meandering for neutral and stable cases reveal comparable results for cutoff frequency and peak frequency. Moreover, the calculated Strouhal number is consistent with values found in the literature of $St = 0.16$. The unstable case shows significant differences, but there is some uncertainty associated to these results. Meandering behavior is largely similar between yawed and non-yawed turbines in the unstable and neutral case, while for the stable case slightly larger amplitudes are observed for the yawed condition. More generally, an increase in stability decreases both amplitude and frequency of oscillations.

Keywords: Wind Turbine, Wake Meandering, Atmospheric Stability, Wake Deflection, Computational Fluid Dynamics

1 Introduction

Offshore wind energy is emerging as the next large scale energy production device, with better economic conditions, technological development and favorable policies opening new markets and areas for production. According to the most recent estimates of the international energy agency (IEA), total offshore wind capacity is set to more than triple by 2026, reaching almost 120 GW of installed capacity, which would account for one fifth of the total capacity of installed wind energy [1].

When more wind farms with bigger turbines are being built offshore, the occurrence and importance of different atmospheric conditions is increasing. This makes understanding how this affects the flow dynamics of wind turbines more important in order to optimize energy production and operation of wind farms.

As mentioned in a review paper by Porté-Agel et al. [2], it has been shown in numerous papers that the convective boundary layer displays stronger wake meandering and faster wake recovery compared to the neutral and stable atmospheric boundary layers [3–10]. Wake meandering is associated with one of the main impacts that stability has on the flows namely changes in length and velocity scales of the atmospheric turbulence. Faster wake recovery is attributed to the increase in turbulence intensity, another consequence of decreasing stability, as found by Abkar and Porté-Agel [9]. They found that not only the magnitude, but also the spatial distribution of the mean velocity deficit, turbulence intensity and turbulent momentum fluxes, were affected. In the present study, the Mann turbulence model is used to replicate different sized eddies in the different inflows and the corresponding spatial coherence.

There are two theories that attempt to explain the meandering of wind turbine wakes. One is that the wake is passively advected by large scale turbulent motion originating from the inflow [11]. The other is an observation that wake meandering behind wind turbines exhibits similar behavior to that of vortex shedding behind bluff bodies in high Reynolds number flows. The non-dimensional Strouhal number represents the frequency associated to this vortex shedding and its expected value for flow around a solid circular disk is around 0.12, the same as for a turbine with a very high tip speed ratio. As tip speed ratio decreases, St increases. Medici et al. [12] found experimentally that for a variety of turbine configurations, St was in the range of $0.12 \rightarrow 0.2$. Trivellato et al. [13] found $St = 0.16$ to be a recurring number both in their Computational Fluid Dynamics (CFD) study of their wind turbine, and in many other studies of seemingly unrelated flows presented in their literature review.

Wake steering shows potential in improving wind farm efficiency and reduce wake losses, both in wind tunnel studies [14] and field campaigns [15]. The research into wake steering under different atmospheric stabilities has not been as extensive as for the non-yawed conditions, with a few notable exceptions. Churchfield et al. [16] performed experimental and numerical measurements at the The Scaled Wind Farm Technology (SWiFT) facility with the aim of measuring wakes and wake deflection resulting from yaw misalignment under a variety of atmospheric conditions. Actuator line large-eddy simulation (AL-LES) simulations are initially run in order to better plan and predict subsequent experiments using light detection and ranging (LiDAR) measurements. These experiments indicated that wake deflection will be strongest under stably to neutrally stratified conditions, and the enhanced mixing of the unstably stratified conditions decreases the amount of expected deflection. Under stable and neutral conditions, a maximum wake deflection of about one third of a rotor diameter is expected 5 rotor diameters(5D) downstream, while this is reduced by roughly half under convective conditions.

In a study by Vollmer et al. [17], an actuator disc large-eddy simulation (AD-LES) representation of the 5MW NREL turbine

[1]Corresponding Author.
June 9, 2023

was simulated under different atmospheric conditions. This study suggested that it might not be reasonable to deflect the turbine wake through yaw in unstable conditions, as no correlation was found between the wake position and turbine yaw angle under convective conditions. In a later PhD thesis by Vollmer [18], wind farm control under different atmospheric conditions using LES was addressed. It was found that parameters such as atmospheric stability, wind veer, shear and turbulence intensity are important parameters to predict the wake deflection of wind turbines, and that wake deflection can increase the energy yield of a two turbine array in a neutral and stable atmosphere, while the same could not be said about a convective atmosphere. Similar results have also been reported in field campaigns by Fleming et al. [19], and in LES simulations by Wei and Wan [20] and Wei et al. [21].

The allure of capitalizing on the potential energy production gains of wake steering has prompted the construction of several analytical models. Analytical models for calculating the wake trajectory of yawed wind turbines have been proposed by Jiménez et al. [22], Bastankhah and Porté-Agel [23], Qian and Ishihara [24] and Shapiro et al. [25], in chronological order. Each model was based on previous work, attempting to improve the accuracy of wake deflection estimates. A mixture of theoretical derivation with different approaches, numerical simulations and wind tunnel experiments were used for development and testing. One of the main distinctions between models is the assumed shape of the distribution of velocity deficit and skew angle, those being a top-hat and Gaussian distribution. The Jimenez model uses the top-hat which is often used to explain why its predictions differs greatly from the others, that use the Gaussian distribution.

Previous work done by the authors tested the effects of yaw misalignment on two different wind turbines. RANS simulations were verified and validated and compared to the analytical wake deflection models described previously [26]. Selected figures and work from that study are included in appendix C.

With the announced increase in energy production from wind farms, understanding the flow dynamics involved allows for more accurate modeling to help with design and optimization. Wake deflection is likely to be viewed as an attractive option within wind farm control. For this technique to mature, however, one of the questions that needs to be addressed further is how the wake behind yawed wind turbines behave in non-neutrally stratified atmospheres, which are dominant offshore, and how well analytical models are able to predict this wake deflection.

This paper intends to investigate the wake dynamics of wind turbines with and without yaw under different atmospheric stabilities. This will be done through large-eddy simulations of the Vestas V80 wind turbine with inflow representing stable, neutral and unstable atmospheres generated using the Mann turbulence generator superimposed onto the wind shear profile. A fast Fourier transform will be performed on the wake meandering, and the energy containing frequencies and wake center position will be studied $8D$ downstream of the wind turbine. Finally, the wake deflection trajectories will be compared with the predictions made by analytical models.

Since these numerical simulations are strictly aerodynamic representations of the wind turbines, the second big question that needs to be addressed for adoption of yaw steering strategies cannot be answered here, namely the structural loads on the wind turbine subject to different wake conditions. Different turbulence generators are not investigated either in the development of this model, and the inflow parameters are based on findings from Riverra-Arreba et al. [27].

2 Turbines

In this work the Vestas V80 and Samsung S7.0-171 turbines are used. The V80 turbine is of interest because it is well described numerically and has relevant validation data available in the literature. The Samsung turbine is currently used for field research at Levenmouth [28], and it is therefore of academic interest to represent it numerically. Some key properties of the turbines are given in table 1. The turbines will be implemented in openFOAM through an actuator line method where the aerodynamic forces of the blade are distributed along a line, which will me implemented in the Navier Stokes Equations (NSE) as a momentum sink term [29]. In this model, neither tower, hub or nacelle are included. Foti et al. [30] investigated the effect of this simplification and concluded that regardless of nacelle, the same results are achieved for velocity deficit in the far wake.

Table 1 Turbine properties for both wind turbines.

	Vestas V80	Samsung S7.0-171
Rated power [MW]	2	7
Number of blades	3	3
Rotor diameter [m]	80	171.2
Hub diameter [m]	3.3	4.2
Blade length [m]	38.35	83.5
Rated wind speed [m/s]	15	11.5
Rated rotor speed [rpm]	19.1	10.6
Hub-height [m]	70	110.6

2.1 Creating Samsung S7.0-171 turbine. A numerical model of the Vestas V80 turbine was already available for the authors, but the same was not true for the Samsung S7.0-171 turbine. Detailed aerodynamic data for the Samsung turbine is not publicly available, and it had to be constructed from turbine performance data from Serret et al. [31] using openFAST with a basis in the well known 5MW NREL turbine [32]. This was done due to the availability field measurements of the turbine wake collected from the Levenmouth turbine through the Total Control project [28]. The changes done to the turbine are summarized in table 2.

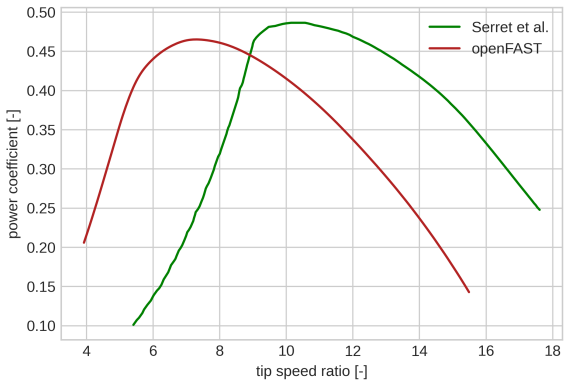

Fig. 1 Power coefficient for different tip speed ratios of the 7MW Samsung turbine.

The c_P-curve of the resulting turbine is presented in figure 1 along with the same curve from Serret et al. [31]. A discrepancy can be seen between the two curves, where the maximum value of the power coefficients occurs at a tip speed ratio (TSR) of around 10 for the reference curve, while the curve produced by the authors gives a max c_P at $TSR = 7.27$. For this case, it was found that when using the c_P curve produced by the authors in openFAST, the thrust and power of the turbine were in agreement with what is reported from literature, with the same not being true when relying on the c_P curve form Serret et al. [31]. This was also found to be true when implementing the turbine in openFOAM later on, see section 5.1.3. The c_P curve produced from openFAST was therefore accepted.

Table 2 Alterations done when creating the Samsung S7.0-171 turbine.

	5MW NREL value	7MW Samsung value
Rotor diameter [m]	126	171.2
Hub diameter [m]	3.0	4.2
Chord increase factor	1.0	1.35
Pitch angle [°]	0.0	−2.5
Tower height [m]	90.0	110.6
Over hang	−5.01910	−7.78

3 Flow analysis

Some key methods of post-processing the data obtained from the numerical simulations and produce figures to analyze results are presented.

3.1 Wake center tracking. How the location of the center of the wind turbine wake in a plane at a given down stream distance is calculated is highly relevant since the path of the wake for different inflow and operating conditions is of great interest. Different methods of finding the wake are described and implemented in python by Quon [33], and illustrated in figure 2 at $8D$ downstream of the Vestas turbine for a neutral atmosphere.

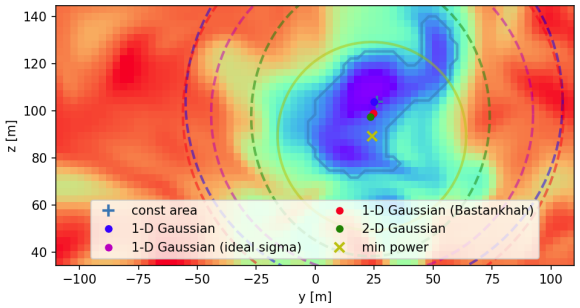

Fig. 2 Contour plot showing the prediction of the wake center for different tracking methods.

The different methods were evaluated through visual inspection at downstream distances from $1D$-$8D$, for the stability cases of unstable, neutral and stable including cases with and without yaw. 1-Dimensional Gaussian (ideal sigma), 1-Dimensional Gaussian (Bastankhah) and the contour-area approaches gave the most accurate and reliable results. The method eventually chosen was the contour area approach, due to its higher consistency. In this method, contours of constant velocity in the plane in question are calculated, and the contour that covers an area that most closely resembles the rotor area, is assumed to represent the turbine wake. The center is given as the geometric center of the contour. This ensures that the estimated wake center is placed in the vicinity of this boundary, which reduces the likelihood of grave errors observed using the other methods.

3.2 Wake deflection. For the yawed turbine simulations, the wake deflection will be compared to the analytical wake deflection models of Jiménez et al. [22], Bastankhah and Porté-Agel [23], Qian and Ishihara [24] and Shapiro et al. [25], using the wake expansion factor estimate described by Carbajo Fuertes et al. [34]. The equations giving the wake deflection estimates can be found in appendix C.

3.3 Spectral analysis. The wake center in the lateral (y-) direction at a fixed downstream position was plotted against time and further analyzed in the frequency, f, -domain by calculating the power spectral density (PSD). The location of interest is $8D$ as it is a candidate for the placement of a new turbine in a wind farm.

In order to reduce noise from wrongly calculated wake centers, all points outside 3σ either side of the hub were removed, σ being the standard deviation. The power spectral density was calculated using the Welch method with a Hanning window. The results were visualized in a log plot that was used to find the cutoff frequency f_c. This is the frequency at which the value of the PSD starts to taper off, shown for the neutral case without yaw in figure 3. It represents the border between the frequencies containing the most energy in the signal which are more relevant to the analysis.

Using a low-pass Butterworth filter with this f_c and plotting the resulting PSD in a non-log plot, it is then possible to identify the single frequency with the highest power density f_{peak}, see figure 17.

Cutoff frequency is also calculated analytically using equations 1 and 2 for comparison. The equations are similar, but one uses rotor diameter D and the other wake diameter D_w. Finally, the Strouhal number St is calculated using f_{peak}.

$$f_{c,r} = \frac{U_{hub}}{2D} \quad (1) \qquad f_{c,w} = \frac{U_{hub}}{2D_w} \quad (2)$$

$$St = \frac{fD}{U_{hub}} \quad (3)$$

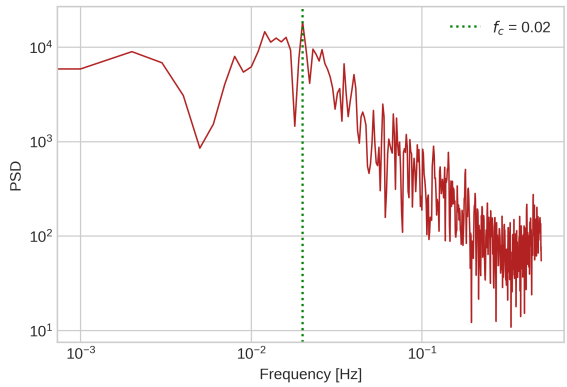

Fig. 3 Log-log plot of PSD for wake meandering and its apparent cutoff frequency, for neutral stability condition for non-yawed turbine.

4 Inflow

The inflow of this study can be broken down into three separate parts, namely shear profile, Mann turbulence model and turbulence intensity.

4.1 Shear profile. The shear profile of the incoming wind velocity will affect the shape and magnitude of the wake. This could be particularly relevant for larger wind turbines since a larger span vertically, means an increase in velocity difference between the top and bottom of the rotor plane. The shape of the shear profile will also be dependent on atmospheric stability. All of these factors necessitates modeling of different shear profiles for the numerical simulations at different atmospheric stabilities. The average wind velocity profile is modeled using the power law in equation 4.

$$U(z) = U_{hub}\left(\frac{z}{z_{ref}}\right)^{\alpha} \quad (4)$$

Here U_{hub} is the wind velocity at hub height, z is elevation above ground, z_{ref} is the hub height and α is an empirically derived exponent that includes both the effects of surface roughness and stability.

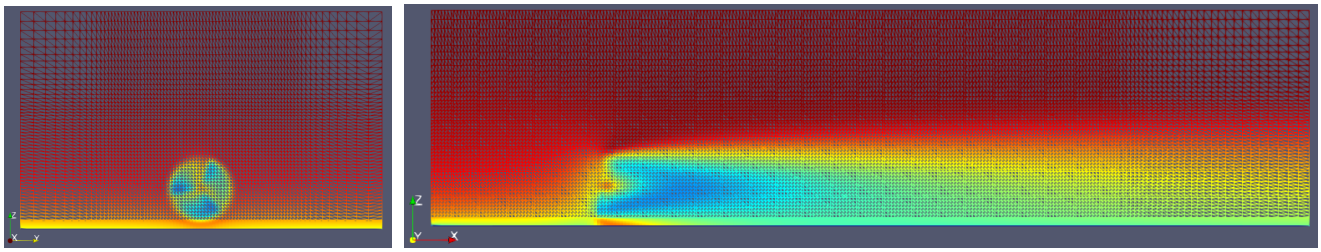

(*a*) (*b*)

Fig. 4 RANS mesh for the Samsung turbine shown in the *(a)* yz-plane and *(b)* xz-plane.

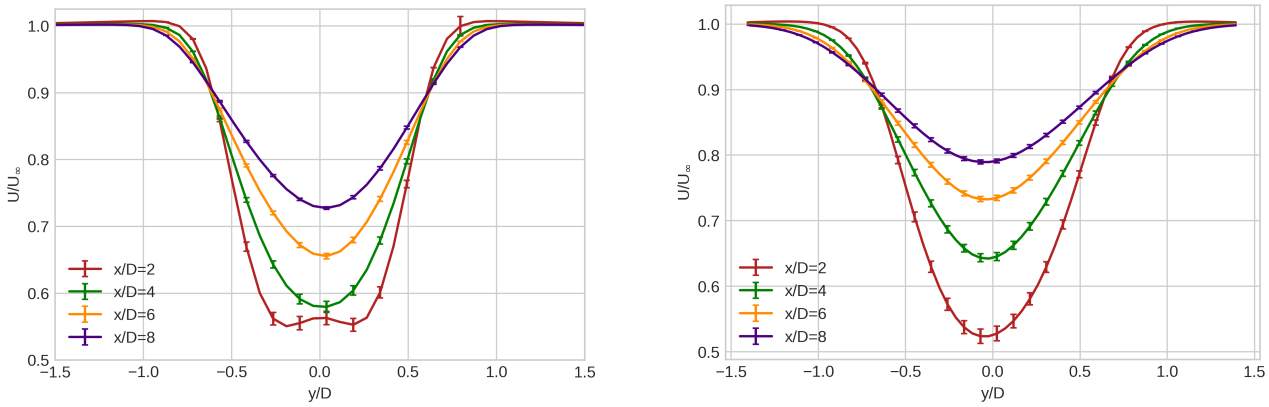

(*a*) (*b*)

Fig. 5 Plot of downstream velocity deficit with error bars from GCI study for *(a)* V80 and *(b)* Samsung turbines.

4.2 Mann model. The Mann spectral tensor attempts to model one aspect of wind field turbulence at an affordable computational cost, namely spatial correlation that occurs due to turbulent eddies. It does this based on the three input parameters: The Kolmogorov constant multiplied by the turbulent kinetic energy viscous dissipation rate to the power of two thirds, $\alpha_k \epsilon^{2/3}$, length scale, L_{Mann}, and the non-dimensional shear distortion parameter related to the lifetime of the eddies, Γ. The resulting output is then a box of specified size containing the fluctuating velocity component at a specified number of points for the x, y and z direction.

Taylor's theory of frozen turbulence allows for an easy conversion between space and time dependent velocity. To quote Taylor [35], *"...one may assume that the sequence of changes in u at a fixed point are simply due to the passage of an unchanging pattern of turbulent motion over the point."*. This means that the longitudinal step size dl_x and total length l_x of the Mann turbulence box can, together with average wind speed, be converted to a time step dt and the total time T respectively.

4.3 Turbulence intensity. The generated fluctuations of the Mann box were also scaled using the specified turbulence intensity TI. It is done by taking the averaged standard deviation of the stream wise wind velocity component of the four grid points closest to the turbine center using all time steps, here denoted σ_1. A scaling factor is then found such that equation 5 is satisfied and subsequently applied to all grid points.

$$\sigma_1 = TI \cdot U_{hub} \tag{5}$$

4.4 Turbulent inflow. For LES simulations, the Mann turbulence generator is used with input parameters based on results found in the literature for offshore conditions at varying stability. The present study used values for $\alpha_k \epsilon^{2/3}$, L and Γ found by Rivera-Arreba et al. [27], where the Mann model parameters were fit to wind fields simulated using LES. Three different wind speeds were simulated for the unstable, neutral and stable conditions. De Maré and Mann [36] found the parameters to be largely independent of wind speed, but not elevation. Values at hub-height were therefore chosen and are presented in table 3.

Table 3 Mann inflow parameters.

	Vestas V80	Samsung S7.0-171
Unstable		
$\alpha_k \epsilon^{2/3}$	0.0419	0.0429
L_{Mann}	80	86.6
Γ	4.4	3.5
Neutral		
$\alpha_k \epsilon^{2/3}$	0.0257	0.0171
L_{Mann}	27.2	33.1
Γ	3.5	3.45
Stable		
$\alpha_k \epsilon^{2/3}$	0.0129	0.0115
L_{Mann}	16.6	13.8
Γ	1.75	1.075

For the y- and z-direction, the length of the turbulence-box exceeds the size of the mesh and the cell lengths are equal to the maximum chord of the turbine blade. Total length and cell size in the x-direction correspond to the total time T_{mann} and time step dt_{mann} defined in the Mann model. They were chosen so that a total time of 3000s could be run, 500s to get past the statistically unsteady ramp-time followed by 2500s of simulation time to reach a converged solution. dt is 0.25s. The effect of cell size and time step of the turbulence box on the solution was not explored in this study, but the values used are similar to other studies such as Rivera-Arreba et al. [27] and Nybø et al. [37].

The generated turbulence was scaled to give the desired TI and the shear profile was superimposed onto it. Again, results from the LES simulations in Rivera-Arreba et al. [27] were used. Table 4 gives their results for α, TI and U_{hub}.

Table 4 Inflow parameters from Rivera-Arreba et al. [27].

	Unstable	Neutral	Stable
α [-]	0.019	0.07	0.146
TI [%]	9.23	4.79	2.91
U_{hub} [m/s]	7.5	7.5	7.5

5 Numerical Simulations

CFD simulations are performed using OpenFOAM in order to analyze the flow dynamics behind wind turbines. The flow field is solved using the OffWindSolver, which is a solver under development by Balram Panjwani at SINTEF Industry [38]. Both RANS and LES simulations are used in this work. The RANS simulations use a RNG (Re-Normalization Group) $k-\varepsilon$ turbulence model, based on the authors' previous experience of this model's suitability for solving wind turbine flows [26]. It models the effect of turbulence as an added viscosity, the effect of which is introduced into the NSEs. Separate transport equations for turbulent kinetic energy k and turbulent dissipation rate ε are solved to find the turbulent viscosity. The RNG $k-\varepsilon$ model is an extension of the standard $k-\varepsilon$ model incorporating additional modifications that work to provide better accuracy in capturing the flow physics and reduce the dependency on user-defined constants. The LES simulations use the Smagorinsky turbulence model to close the NSE equations [39]. The Smagorinsky turbulence model is a method used in LES to approximate the effects of the unresolved small-scale turbulence on the simulated larger-scale flow. It is also an eddy viscosity model and therefore assumes the turbulent stresses are proportional to the local deformation of the flow. Their magnitude is determined using the Smagorinsky coefficient. Its value is usually based on empirical or theoretical considerations, and it affects the accuracy of the model.

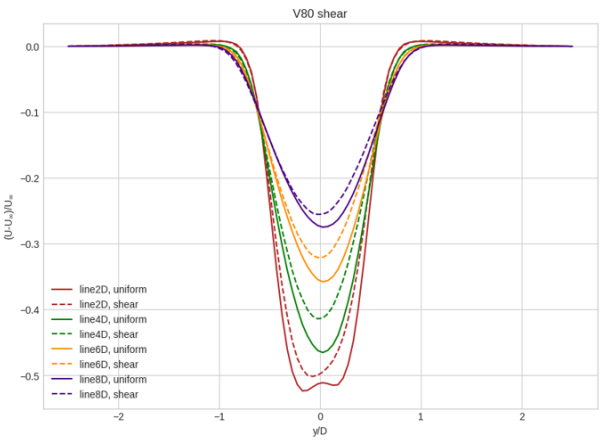

Fig. 6 V80 velocity deficit at different downstream locations in uniform and sheared inflow.

5.1 RANS simulations. RANS simulations were initially run in order to verify and validate the wind turbine models used for this study, in addition to being a building block towards the higher fidelity LES simulations.

5.1.1 Mesh description. Mesh parameters are given in table 5 along with pictures of the mesh in figures 4(*a*) and 4(*b*) for the Samsung turbine. L_i is the domain length and N_i the number of cells in the $i = x, y, z$ directions. $dl_{turbine}$ refers to the cell-size-lengths, which are equal in the x, y and z direction, in the region of the mesh where the turbine is located. Near the ground the cells are refined enough to capture and maintain the inflow shear profile, whilst at the top and back cells are expanded. This reduces computational cost in the regions that are of less importance.

Table 5 Mesh parameters for RANS simulations.

	2MW Vestas V80	7MW Samsung
L_x, L_y, L_z [m]	1400, 500, 250	2435, 1000, 600
N_x, N_y, N_z	190, 61, 55	241, 81, 71
$dl_{turbine}$ [m]	6.0	9.0

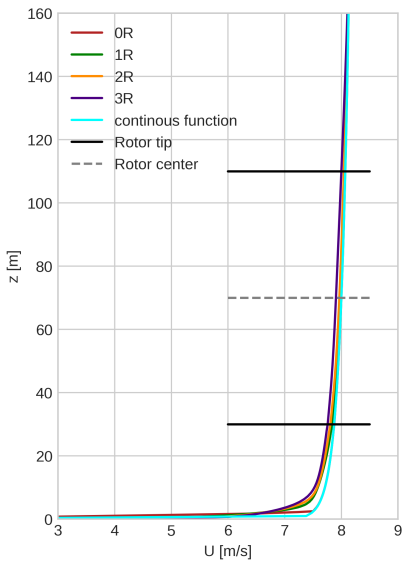

Fig. 7 Shear profiles plotted for locations downstream of the inlet in the V80 RANS simulation used for validation.

5.1.2 Verification. A total run-time of 700 and 1500 seconds for each simulation proved to give a converged solution with respect to time for the Vestas and Samsung turbines respectively. A case with reduced time-step was also run to check the simulations sensitivity to a reduction in residuals. It showed to have minimal effect on both wake, thrust and power for both turbines. Residuals along with results for velocity deficit, turbine thrust and power and time convergence can be found in appendix A.

A mesh refinement study was performed to ensure that grid convergence for the RANS simulations were achieved. Three meshes of increasing refinement named coarse, orig and fine were initially run for both turbines with minimum cell length dx in the refined region. The cell length dx was changed by a factor of $r = 1.25$ between each mesh for the Vestas turbine and $r = 1.33$ for the Samsung turbine. Based on these results a fourth mesh, named medium, with a refinement level in between coarse and orig was proposed and verified for the V80 turbine, while the orig mesh was deemed adequate for the Samsung turbine. Figures 5(*a*) and 5(*b*) show the results of a GCI study performed using the medium and fine meshes, while output for power and thrust from the rotors are presented in table 6.

Shear in the inflow profile proved to have a pronounced effect on the velocity deficit in the wake, as can be seen in figure 6. The shear profile was therefore included in subsequent iterations of the models. A no-slip boundary condition and wall functions were applied at the bottom wall and, in order to capture the steep

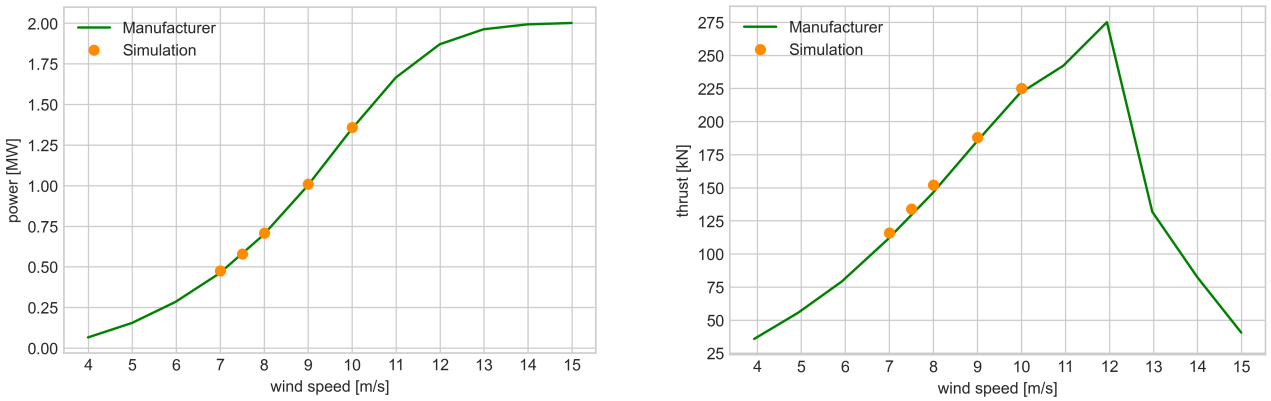

(*a*) (*b*)

Fig. 8 Simulated *(a)* power and *(b)* thrust for the Vestas turbine plotted against curves given by the manufacturer.

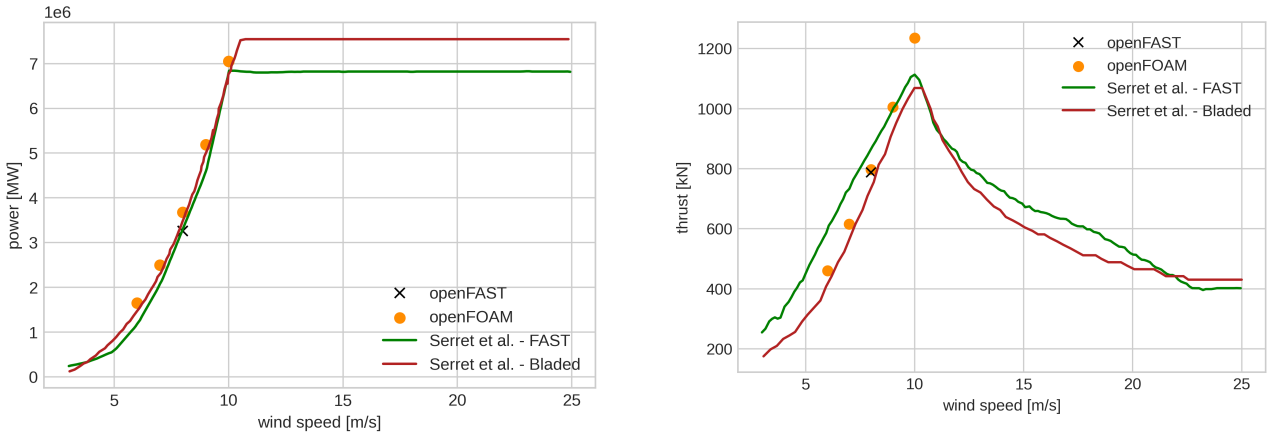

(*a*) (*b*)

Fig. 9 Simulated *(a)* power and *(b)* thrust for the Samsung turbine plotted against curves found in literature.

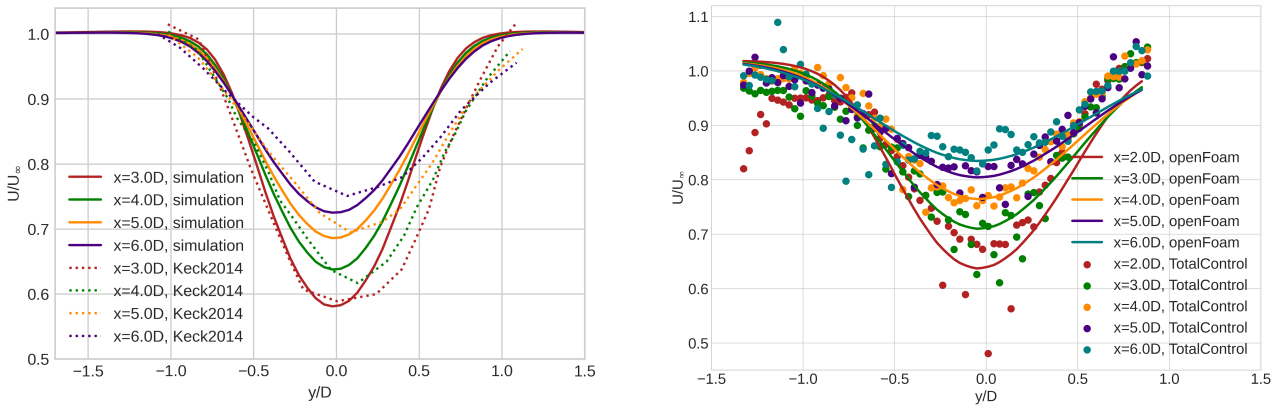

(*a*) (*b*)

Fig. 10 Velocity deficit curves of the *(a)* V80 and *(b)* Samsung turbines at different downstream locations plotted against validation data.

gradient, cells were refined in this lower region. A sufficiently low value for the non-dimensional wall distance y+ needed for an accurate near wall solution was never achieved. However, a plot of the wind velocity profile for locations downstream of the inlet and upstream of the turbine show good agreement with the input velocity profile, especially in the region where the turbine operates, see figure 7. This analysis was done for the Vestas turbine because of the availability of inflow data from Keck et al. [7]. Changes based on the analysis were made to both turbine models.

5.1.3 Validation. RANS simulations in uniform inflow were run at different wind speeds to validate turbine thrust and power.

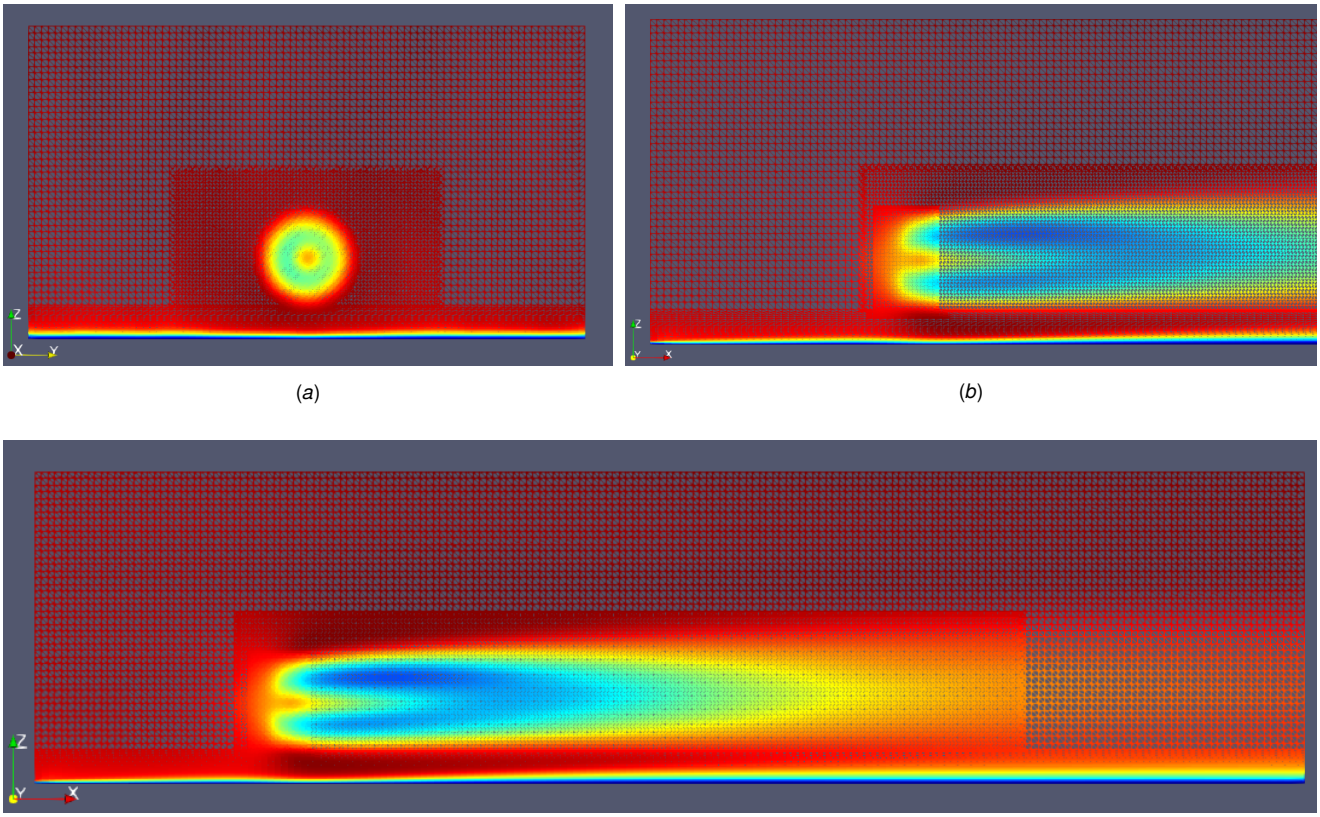

(*a*) (*b*) (*c*)

Fig. 11 Mesh used in LES simulations for the Vestas turbine, *(a)* yz-plane, *(b)* zoomed in on xz-plane and *(c)* wide view of xz-plane.

Table 6 Turbine thrust and power for RANS refinement study.

	Thrust [kN]	Power [MW]
Vestas_{medium}	146	0.791
Vestas_{fine}	148	0.809
Vestas_{Diff}	1.37 %	2.28 %
Samsung_{medium}	790	3.58
Samsung_{fine}	803	3.74
Samsung_{Diff}	1.57 %	4.40 %

The results were compared to performance data given by the manufacturer and found in literature and are given in figures 8 and 9. It can be seen in these figures that both thrust and power are modeled accurately. In figure 9(*b*) it can be seen that at a wind speed of 10 m/s the thrust is overestimated. This is likely because the turbine would approach rated wind speed, and go into a different operating region, which would mean altering the TSR. Tip speed ratio for the V80 turbine is $TSR = 7.3$ and for the Samsung it is as described earlier in section 2.1.

LES data from Keck et al. [7] of a Vestas V80 turbine was used to validate the wake of the RANS case. Keck et al. [7] used a hub-height wind speed of $U_{hub} = 8$m/s in an unstable atmosphere with turbulence intensity $TI = 6.16\%$. A shear profile for the RANS simulation was generated with the power law using $\alpha = 0.019$ as found by Rivera-Arreba et al. [27] for an unstable atmosphere, see table 4. Another parameter with significant impact is the turbulent dissipation rate ε prescribed at the inlet. It is based on a turbulent length scale Tu_L. Setting $Tu_L = 9.5$ gave best agreement with validation data, see figure 10(*a*), and will be used in further simulations. The Samsung turbine was validated with LiDAR data from the TotalControl project [28], where measurements are done on the Levenmouth turbine operated by ORE Catapult. A rather large turbulent length scale of 85.6 meters, or $1R$ (1Radius), gave a solution most similar to that of the validation data, as shown in figure 10(*b*). It should be noted that the data used to validate this turbine is quite noisy, and there is an absence of information describing the inflow conditions when the measurements were made. With a basis in the information given from the TotalControl project, a wind speed of 8m/s and a turbulence intensity of 10% was therefore assumed, while the shear profile was imposed in a similar manner to that of the Vestas turbine.

5.2 LES. A higher fidelity simulation was run using LES for the 2MW Vestas V80 turbine. It was verified and then validated using the same data as previously from Keck et al. [7] before being used to generate results. The Samsung turbine was not used for the LES simulations primarily due to lack of validation data, as explained in section 5.3. For the results, six simulations were run, namely with and without a yaw angle of 20° for each of the three stability conditions presented earlier in section 4.4.

5.2.1 Mesh description. The new mesh has the same domain and cell size as the one used for RANS, only with added refinement regions around the turbine and wake. The mesh was also changed to be uniform in the x, y- and z-directions. The refinement regions were created using openFOAM utility `snappyHexMesh` and the resulting cubic cells are described in table 7. Pictures of the mesh are presented in figure 11. For the simulations of yawed turbines, both wake refinement regions were moved $30m$ in the negative y-direction and the turbine refinement region was expanded $13m$ in front of and behind the turbine. This ensures that both the turbine and the wake are still well captured by the finer cells. Due to the

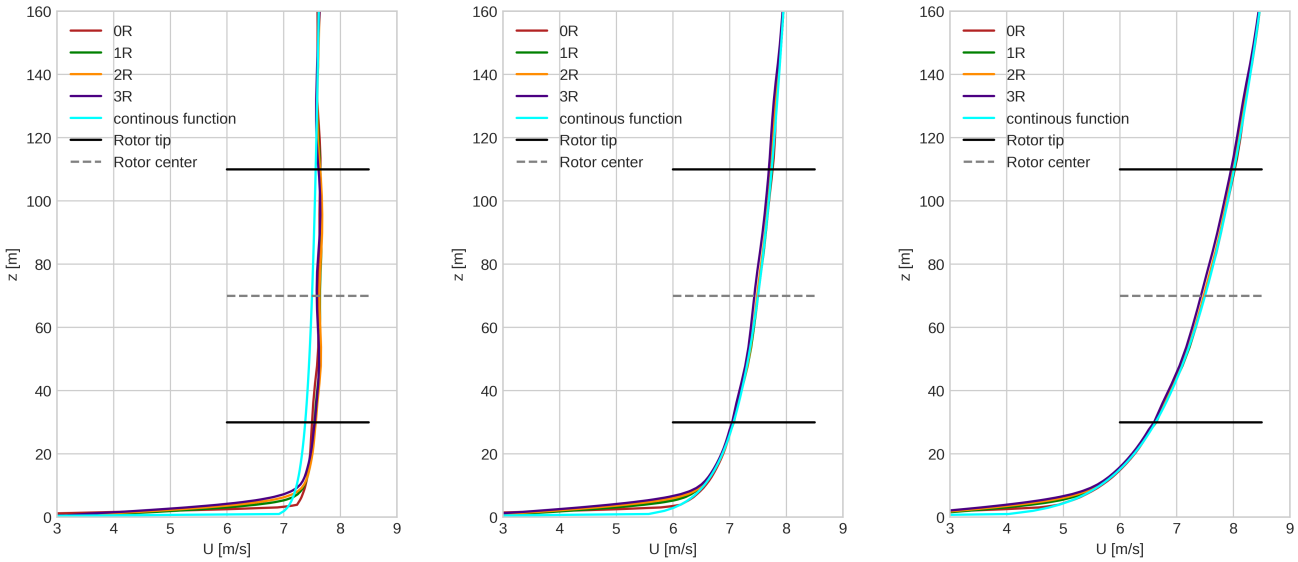

Fig. 12 Inflow shear profiles at locations downstream of inlet for V80 LES simulations in *(a)* unstable, *(b)* neutral and *(c)* stable atmospheres.

angle of the turbine, the wind velocity experienced by the rotor is decomposed by the cosine of the yaw angle. With the new wind speed assumed to be the component normal to the plane of the turbine, a new rotational speed was calculated keeping the tip speed ratio constant.

Table 7 Cell sizes for the various refined regions of the LES mesh.

	Turbine	Wake	Elsewhere
dl [m]	6.0	3.0	1.45

5.2.2 Verification. A simulation was run on a finer mesh with the number of cells increased by a factor of $r = 1.2$ in the x, y and z directions. The two solutions were then used to calculate the grid convergence index for the velocity deficit downstream of the turbine. Along with values for turbine output, the GCI study shows that a finer mesh is not needed, see figure 13 and table 8.

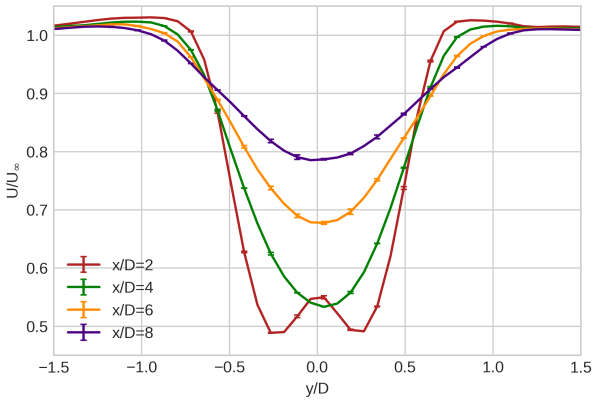

Fig. 13 Plot of downstream velocity deficit with error bars from GCI study for LES simulations of the V80 turbine

Table 8 Turbine thrust and power for LES refinement study.

	Thrust [kN]	Power [MN]
$V80_{medium}$	151.2	0.728
$V80_{fine}$	151.2	0.729
Diff [%]	0	0.1

A total run time of 3000s proved to give a converged solution with respect to wake, thrust and power. A case with a halved time step of $dt = 0.05$ was run to test the models sensitivity to this parameter. This also had the effect of lowering the residuals. Results show that $dt = 0.1$ and the corresponding residuals are sufficiently low which is shown in appendix A.

Both shear profile and turbulence intensity of the simulation were checked for positions upstream of the turbine. It is shown in figure 12 that shear profiles for all positions and stabilities gave good agreement with the desired shear-profile shape. Upon inspection, turbulence intensity was found to decrease substantially from the inlet to turbine. To correct for this, intensity at the inlet was increased. Table 9 gives an overview of the achieved and target values for turbulence intensities.

Table 9 Average turbulence intensity in the inflow of the Vestas V80 turbine for LES simulations, all values are given in [%].

	Inlet	Turbine	Target
Unstable	12.4	9.73	9.23
Neutral	7.75	4.64	4.79
Stable	5.1	2.81	2.91

In addition to the parameters presented above, a number of other simulations were run in order to examine the numerical models sensitivity and reliance on these parameters. This included comparing the Smagorinsky and a dynamic one equation eddy-viscosity turbulence models, testing for different values for the Smagorinsky coefficient, examining different damping functions within the Smagorinsky model and running a simulation with a larger domain. Of these, it was found that the turbulence model, the Smagorin-

sky coefficient and extended domain influenced the solution to a very small degree. The choice of damping function provided in openFOAM did impact the solution more, and among the Prandtl, van Driest and cube-root volume damping functions, the simpler cube-root volume damping functions were shown to give results most representative of the validation case.

5.2.3 Validation. Simulated turbine thrust and power for all stabilities at 0 degrees yaw are compared with values from the turbine manufacturer given in table 10. The wake deficit is then compared with Keck et al. [7], following the same procedure as in section 5.1.3, and presented in figure 14. Ideally, field measurement data or a higher fidelity model would be used to validate this LES model, thereby avoiding one LES model being used to validate another LES model. Time restrictions and data availability made this unachievable, but the validation results are an indication of a realistic turbine wake nonetheless.

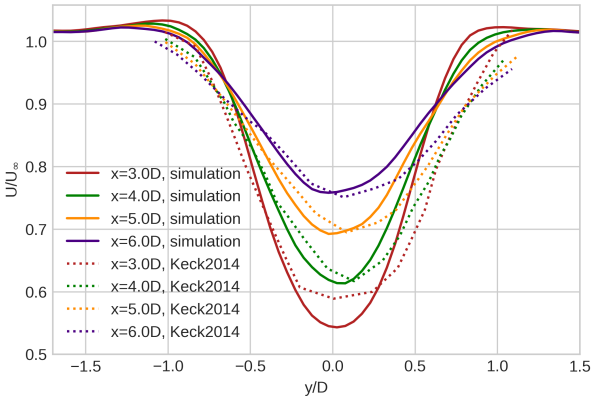

Fig. 14 Velocity deficit curves of the V80 turbine for LES simulations at different downstream locations plotted against validation data from Keck et al. [7].

Table 10 Validation of turbine thrust and power for V80 LES simulations.

	Thrust [kN]		Power [MW]	
	Simulated	Target	Simulated	Target
Manufacturer	150.8	151	0.732	0.710
Unstable	132.1	132	0.607	0.600
Neutral	133.0	132	0.593	0.600
Stable	133.3	132	0.591	0.600

5.3 Samsung Turbine. As previously stated in sections 2.1 and 5.1.3, the numerical Samsung turbine match the performance expected from literature well. Even though the LiDAR measurements are noisy, the wake of the Samsung turbine was able to replicate the measured data to a reasonable degree with a turbulent length scale of one rotor radius for the RANS simulations (figure 10(*b*)). For future implementations of the turbine, the tilt angle should be smaller. The value of this parameter followed from the 5MW NREL turbine and was not altered. It can be seen in figure 4(*b*) that the wake and wake center of the turbine has a downwards trajectory, which is likely due to this high tilt angle. The wake center not going parallel to the horizon could also be a reason as to why this turbine needs such a high turbulent length scale to match the validation data.

Ultimately, however, the choice was made to use the V80 Vestas turbine in favor of the Samsung S7.0-171 turbine. This came down to the fact that for the Vestas turbine, the validation data was given for well described inflow conditions, while the same could not be said for the Samsung turbine. Seeing that in many cases the wind speed was not well defined, and that the turbulence intensity was not specified for any of the measurements, the authors could not validate the turbine with sufficient confidence to pursue high fidelity LES simulations aiming at investigating the influence of atmospheric conditions on the flow.

However, the rotor performance of the turbine compares well with literature and the RANS simulations gives reasonable agreement with the TotalControl data. Other publications may therefore find the information useful, especially with access to validation data with a better description of the inflow.

6 Results and discussion

6.1 Wake deficit. Figure 15 shows the wake deficit for all atmospheric conditions for the Vestas turbine at different downstream locations. As expected, the deficit is larger for the stable atmospheric condition followed by neutral atmospheric condition, while it is significantly smaller for the convective atmosphere. At $6D$ and $8D$, the wake has reached 85% and 90% of the free stream velocity respectively for the unstable atmospheric conditions. During inspection of the wake meandering for the this stability, it was also found that the wake tracking algorithm had trouble finding a well defined wake center for all surfaces greater than $4D$. Considering these factors, there is reason to believe the wake is all but dissipated beyond $4D$, while it is still very much present for the neutral and stable atmospheres. This is also in line with findings from literature [2].

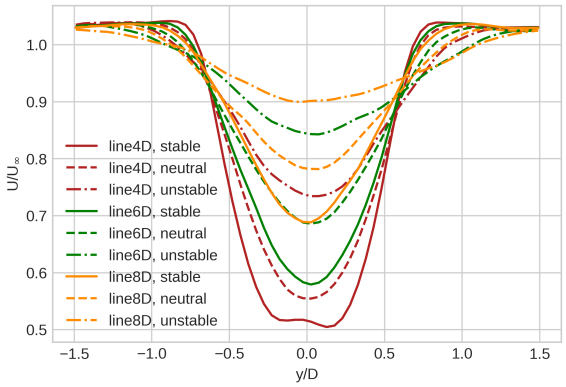

Fig. 15 Wake deficit for Vestas V80 for all atmospheric conditions at $4D$, $6D$ and $8D$.

6.2 Wake deflection. The wake deflection is shown in figure 16 by finding the wake center as described in section 3.1 using the averaged velocity from the LES simulations. It is also plotted for the averaged position of the wake center at each downstream surface for the entire time series, with time steps sizes of 1 and 10 seconds. Filtering based on standard deviations, described in section 3.3, is applied to the meandering signals such that the wake center measurements that are clearly unphysical are removed, while keeping as much of the original measurements as possible. The deflection is then plotted against the analytical wake deflection models of Jiménez et al. [22], Bastankhah and Porté-Agel [23], Qian and Ishihara [24] and Shapiro et al. [25]. The equations used in these models are specified in the appendices.

Comparing at the wake deflection for the neutral and stable atmospheres in figures 16(*a*) and 16(*b*), they appear to be very similar. The greatest difference between the simulated deflection using the mean velocity field of the numerical solutions is found to be 2m at $2D$ downstream. For the analytical solutions, the biggest differences are in the far wake, and are found to be just under 5m for

Jimenez's model, around 2m for Shapiro's model slightly less than 1m for the two remaining models. These findings are in agreement with the findings of Churchfield et al. [16] and the maximum wake deflection of about one third of a rotor diameter at $5D$ found in that paper, is in excellent agreement with the deflection of 23.5m or 0.29 rotor diameters found in the

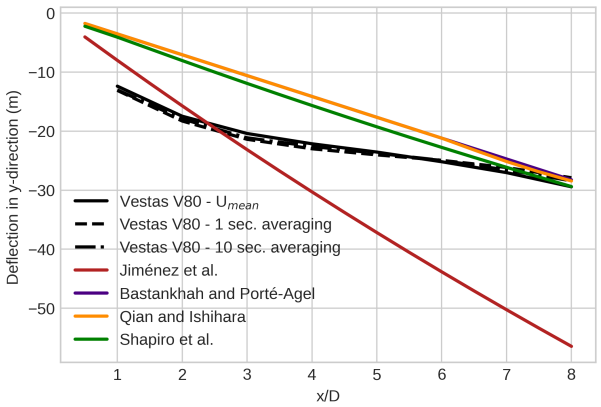

(*a*)

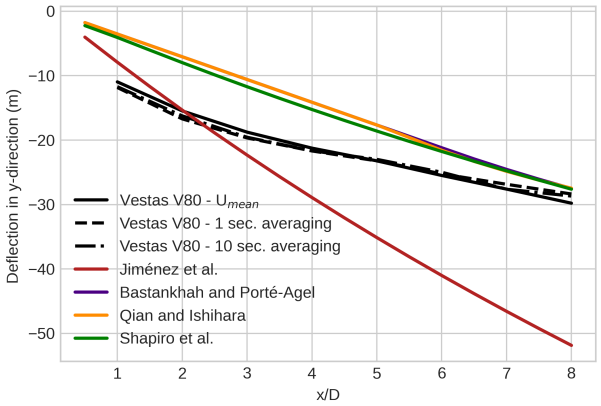

(*b*)

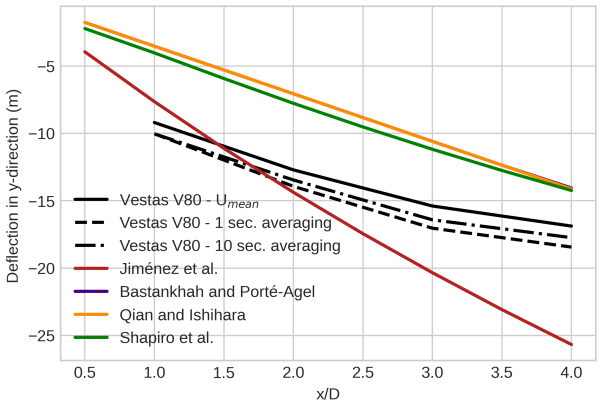

(*c*)

Fig. 16 Wake deflection for Vestas V80 compared to analytical models, shown for *(a)* stable, *(b)* neutral and *(c)* unstable atmospheric conditions.

current results. The reduction of deflection by roughly half for the unstable case is not observed for the deflection shown in figure 16(*c*). It should be noted that due to the difficulties locating a wake center in the far wake of this turbine, the results are only shown until $x = 4D$. Further downstream at $8D$, the wake deflection increases to roughly $0.37D$ in the lateral direction. It can be seen in figure 15 that at $8D$ downstream, the wake is around 2 diameters wide. This means that the mean wake will still heavily interfere with a downstream turbine, and that this turbine would be in partial wake conditions. If the meandering at $8D$ downstream is also considered from figure 17 this indicates that this wake would oscillate with a magnitude of 0.25 rotor diameters in both directions, which could induce additional unsteady loads on a downstream turbine. Seeing that the wake produced by the unstable atmosphere is found to be largely dissipated beyond $x/D = 4D$, and since there is little reason for deflecting a dissipated wake away from downstream turbines, it does appear that it would be less attractive to deploy wake steering strategies in an unstable inflow.

Continuing with a comparison between the simulated and analytical wake trajectories, it can be seen that the initial wake displacement is greater for the numerical solution. The deflected wakes then follow a more gentle slope to the far wake where a better agreement with the analytical solutions are found, and at $8D$ a good estimate is achieved for all models but Jimenez's. It is interesting that the wakes of the more stable atmospheres appear to have a greater initial wake displacement than that of the unstable atmosphere. This could indicate that initial wake displacement decreases with decreasing atmospheric stability, but more research is necessary to say anything conclusive.

It was found in the project assignment [26] using a uniform flow RANS simulation without shear, that the trajectories of the analytical solutions then followed the trajectories of the simulated wake displacement to a excellent degree, as can be seen in appendix C. The differences between these simulations and the current ones are the turbulence model, turbulence intensity and inflow profile. A subject for further work on these models could therefore be to investigate which of these parameters impact the wake deflection the most. Focusing now on the wake deflection plotted for different averaging times, it is seen that they all follow similar trajectories. The 1 and 10 second averages are found by using the average wake position over the wake center for each surface for the entire time series, which indicates that the meandering of the wake occurs around the deflected wake axis.

Table 11 Results from spectral analysis, all frequencies f^* are given in [s^{-1}].

	$f_{c,r}$	$f_{c,w}$	f_c	f_{peak}	St [-]
Unstable	0.0469	0.0276	0.0108	0.0069	0.0736
Neutral	0.0469	0.0234	0.02	0.0120	0.1632
Stable	0.0469	0.0276	0.0275	0.0153	0.1707

6.3 Wake meandering. For the neutral and stable stabilities, meandering is analyzed 8 diameters downstream of the turbine, at $x = 8D$. As the unstable case had no clearly defined wake at this location, see section 6.1, it was necessary to use $x = 4D$.

The Welch method was used with a Hanning window and 1024 samples per segment with an overlap of 50% for the window-averaging. The total duration of the time-series is 2500s and the sampling frequency is $f_s = 1s^{-1}$. Using the method described in section 3.3, results for cutoff frequency f_c (see figure 3) and peak frequency f_{peak} were obtained and are presented in table 11. $f_{c,w}$ and $f_{c,t}$, the analytical versions of f_c calculated with equations 1 and 2, are also given in the table along with the Strouhal number St calculated using equation 3.

Figure 17 shows the low pass Butterworth filtered wake position for a fixed point over time and its corresponding PSD for all stabilities with and without yaw. For the unstable and neutral case, the meandering is very similar for the yawed and non-yawed turbine, whilst for the stable case the yawed turbine appears to give a slightly larger meandering amplitude. Comparing stability conditions, amplitudes for unstable simulations appear to be larger than

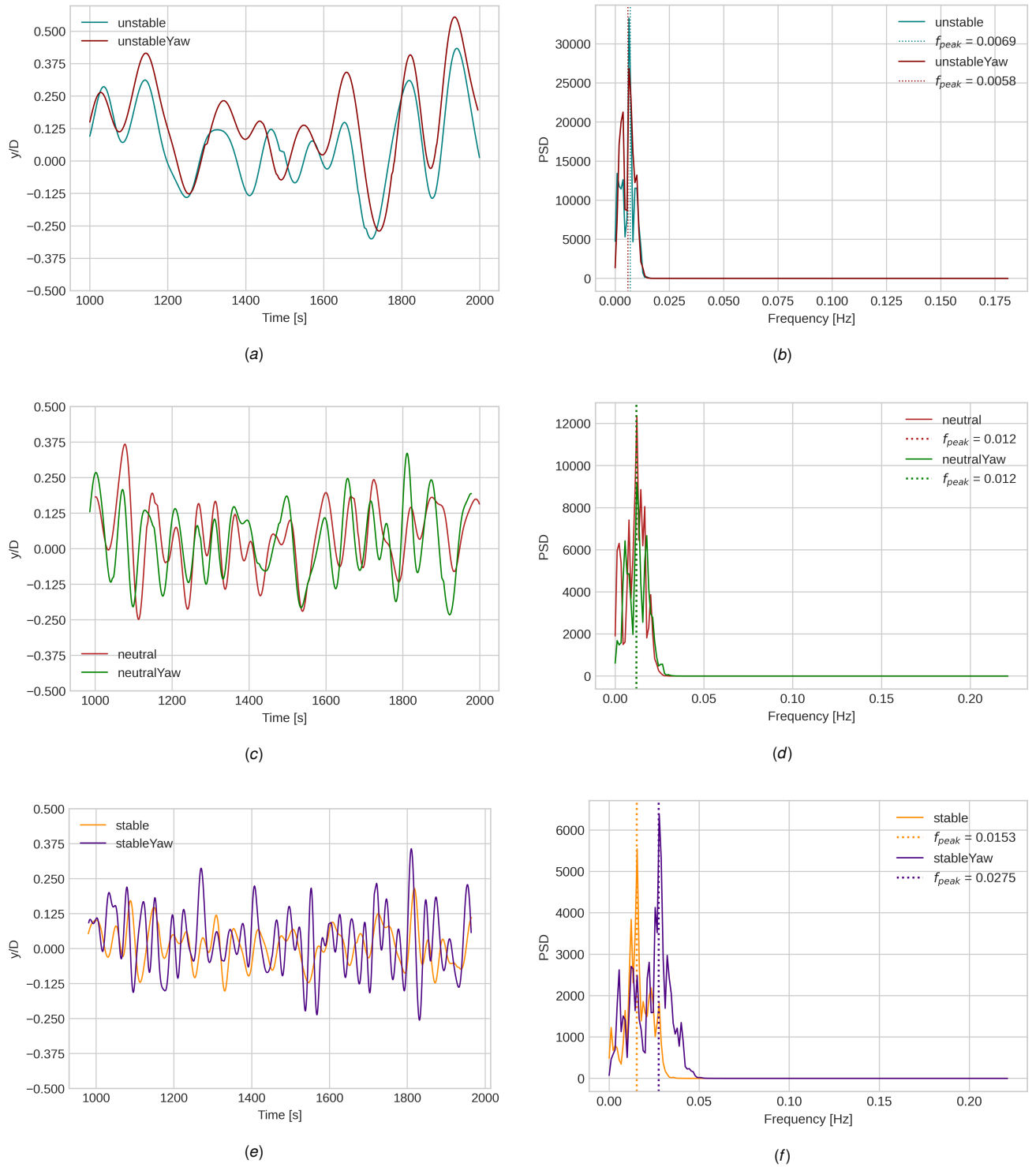

Fig. 17 Meandering (left) and low-pass filtered PSD (right) plots for unstable (top), neutral (middle) and stable (bottom) atmospheres.

neutral and neutral are again larger than stable, but perhaps only in non-yawed condition. The frequency of oscillations for the meandering looks to decrease with increasing stability regardless of yaw, which is supported by results for peak frequency in figures 17(*b*), 17(*d*) and 17(*f*).

Although the unstable case uses wake centers at a different downstream location ($4D$ and not $8D$), results for f_c, f_{peak} and St at $4D$ downstream in the neutral and stable cases gave similar results to $8D$, see appendix B. This indicates that results of this kind are somewhat independent of downstream position.

Results for stable and neutral inflow agree quite well with the analytical cutoff frequency calculated using the wake diameter, $f_{c,w}$. In regards to the Strouhal number findings for the stable and neutral case are consistent with values found by Medici et al. [12] and Trivellate et al. [13] of $St = \langle 0.12 \rightarrow 0.2 \rangle$ and $St = 0.16$ respectively.

St for the unstable case is significantly lower. The result could indicate that for convective inflow, bluff body dynamics no longer

apply to the meandering motion. Instead it could be the result of the wake deficit being advected passively by the larger eddies in the inflow. A lower peak frequency is reminiscent of the lower frequencies, representative of the larger eddies, dominating the power spectral density of convective inflows. However, considering the limitations of the model and the difficulties faced when finding the wake center for this case, the large difference in St warrants further inspection and verification before any conclusions can be drawn.

7 Conclusions

Understanding the impact of atmospheric conditions on wind turbine flow dynamics is crucial for optimizing energy production and operational efficiency. Offshore wind farms introduce challenges related to larger turbines and different operating conditions. The effect of atmospheric stability on wind turbine wake dynamics has been examined in this work, in particular wake deflection and meandering. High fidelity numerical AL-LES simulations with Mann generated turbulent inflows were used to investigate three different stabilities for turbines with and without yaw.

An attempt was made to reproduce and use the Samsung S7.0-171 in the study. A successful creation of a numerical representation of the turbine has been achieved, which can be useful for later studies. However, due to a high degree of uncertainty in some parts of the validation data that are important for this work, sufficient accuracy of the AL-LES model could not be guaranteed and the Vestas V80 turbine was used instead.

As anticipated, with increasing atmospheric stability and a consequent decrease in turbulence intensity, the wake deficit also increases. Despite these differences observed for wake deficit between the neutral and stable cases, they have very similar deflected wake trajectories when the turbines are in yaw. Both exhibit a greater initial wake deflection than what is expected from the analytical wake deflection models, but this initial sharp gradient flattens out, and at $8D$, good agreement is found between the numerical and analytical results. Beyond $4D$, the turbine wake in the unstable atmosphere has practically dissipated, as indicated by the small wake deficit and challenge in locating the wake center. These findings suggest that wake deflection may not be advantageous in unstable atmospheres, which aligns with the findings of previous research by Vollmer et al. [17], [18]. At $5D$, the wake center position was found to be $0.29D$ which is in excellent agreement with Churchfield et al. [16], who reported a deflection of $0.33D$ for the same downstream distance. In the furthest wake position examined, at $8D$, deflection increases marginally to $0.375D$, exposing a new potential turbine at this location to partial wake conditions. The effect of this is made more substantial when considering that the oscillating motion from meandering has a magnitude equal to $0.25D$. It was also found that the wake trajectories were very similar if the mean velocity was used to find wake centers, or if the wake center position was found using the mean value of the meandering wake. This would suggest that the meandering behind yawed turbines occur around the deflection axis.

Meandering analysis was conducted at $8D$ for neutral and stable stabilities, while the unstable case used $4D$ due to the absence of a clearly defined wake. The Welch method with specific parameters provided results for cutoff frequency, peak frequency, and Strouhal number. In the neutral atmosphere, meandering behavior was similar between yawed and non-yawed turbines, while slightly larger amplitudes were observed for yaw compared to non-yaw in the stable case. Neutral simulations exhibited larger amplitudes compared to stable, non-yawed simulations. Meandering frequency appeared higher in both stable cases, supported by the peak frequency results. Results at 4D in the neutral and stable cases were similar to those at 8D, indicating some independence from downstream position. The results for stable and neutral inflows aligned well with the analytical cutoff frequency using the wake diameter. Strouhal number findings were consistent with previous studies for stable and neutral cases, but significantly lower for the unstable case. This could suggest different dynamics, however, considering the model limitations and challenges in determining the wake center, further inspection and verification are needed to draw conclusive insights.

Acknowledgments

First and foremost, we would like to express our deep gratitude to Balram Panjwani and Tania Bracchi. We are very fortunate to have had such dedicated supervisors. Their wealth of knowledge, guidance and personal touch have been invaluable throughout this project. We would also like to offer a special thanks to Irene Rivera-Arreba. The work of her and her colleagues was fundamental to this study. Additionally, Irene's willingness and patience in answering questions related to a challenging topic is much appreciated. Finally we would like to recognize the Idun high-performance computing platform as an essential resource for our numerical computations.

Appendix A: Verification

A.1 Residuals, RANS. Residuals for the Vestas RANS simulations are presented in figure 18. A decrease in residuals is seen for the simulation with reduced time step.

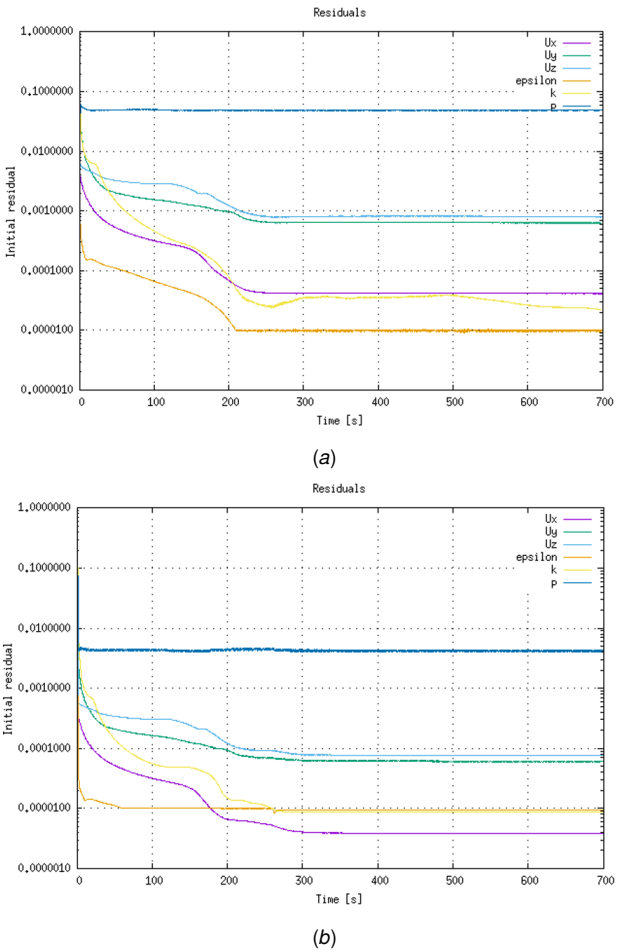

Fig. 18 Residuals for the RANS reference case *(a)* and reduced time step case *(b)*. dt = 0.1 and dt = 0.01 respectively.

A.2 Run-time convergence, RANS. Velocity deficit for the V80 (figure 19) and Samsung (figure 20) RANS simulations run for different lengths of time in order to decide converged time step.

The figures show that convergence is reached at 1500 seconds for the Samsung turbine and at 700 seconds for the Vestas turbine. Turbine thrust and power converged at around 200-300s, long before the wake.

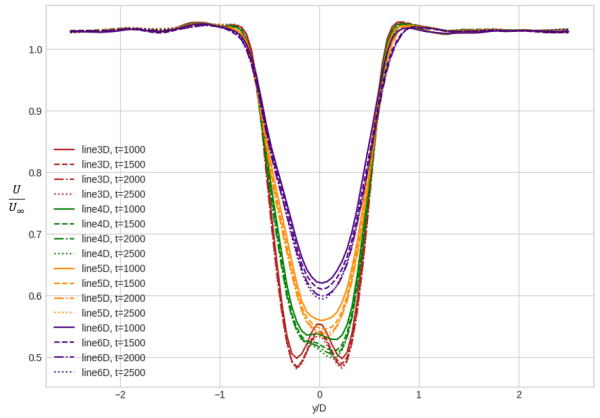

(*a*)

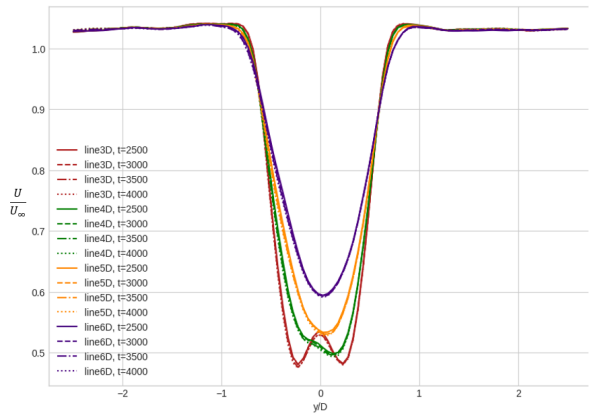

(*b*)

Fig. 19 Plot of velocity at hub height for different downstream locations and run-times, V80 RANS.

A.3 Reduced time step, RANS. Results for the V80 and Samsung RANS simulations using two different time steps $dt = 0.1$ and $dt = 0.01$ are shown. Velocity deficit in the wake is in figure 21(*a*) and turbine thrust and power are found in table 12.

Table 12 Turbine thrust and power for refinement study for the Vestas turbine, V80 RANS

	Power [MW]	Thrust [kW]
$dt = 0.1$	152	0.710
$dt = 0.01$	151	0.721
Diff [%]	0.6	1.5

A.4 Residuals, LES. Residuals for the V80 LES simulations are presented in figure 22. A decrease in residuals is seen for the simulation with reduced time step.

A.5 Run-time convergence, LES. Velocity deficit for the Vestas V80 LES simulation are run for different lengths of time in order to decide converged time step. 3000 seconds was determined to be sufficient run time, the thrust and power converged long before the wake.

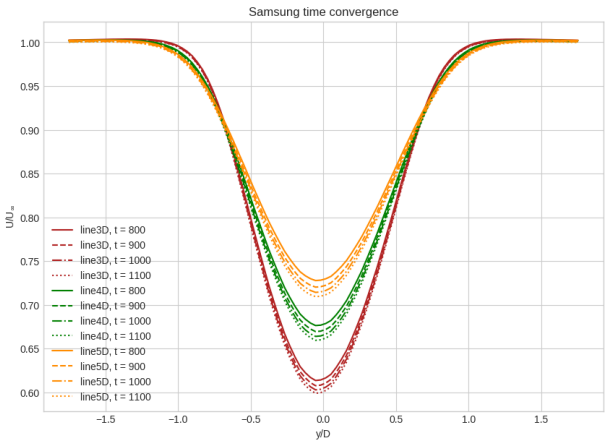

(*a*)

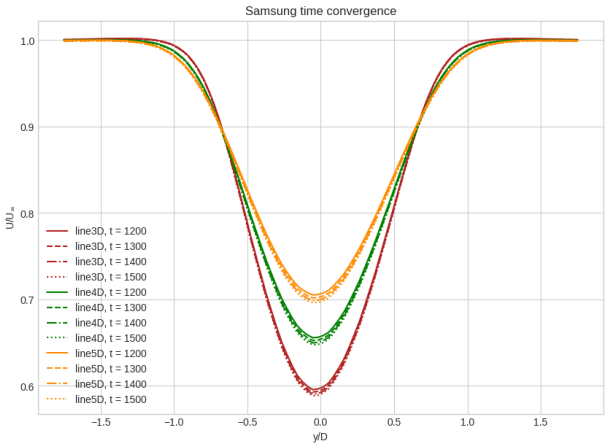

(*b*)

Fig. 20 Plot of velocity at hub height for different downstream locations and run-times, Samsung RANS.

A.6 Reduced time step, LES. Results for the V80 LES simulations using two different time steps, $dt = 0.1$ and $dt = 0.05$. Velocity deficit for wake is in figure 24 and turbine thrust and power are shown in table 13.

Table 13 Turbine thrust and power for refinement study, V80 LES

	Power [MW]	Thrust [kW]
$dt = 0.1$	151.2	0.728
$dt = 0.05$	150.9	0.719
Diff [%]	0.2	1.2

Appendix B: More spectral analysis

Results from spectral analysis of meandering $4D$ and $8D$ downstream of the turbine for the neutral and stable cases are shown in table 14. They show strong similarities to each other.

Appendix C: Analytical wake deflection models

The following section is adopted from the project assignment of the authors [26].

Jiménez et al. [22] derived equation C1 for the skew angle where deflection is determined by integrating with respect to x. It assumes a uniformly distributed velocity profile inside the velocity deficit region, known as the top-hat assumption.

Table 14 Average turbulence intensity for v80 LES inflow.

	Neutral	Stable
$f_c\,[s^{-1}]$		
$4D$	0.02	0.0265
$8D$	0.02	0.0275
$f_{peak}\,[s^{-1}]$		
$4D$	0.016	0.016
$8D$	0.012	0.0153
St [-]		
$4D$	0.1707	0.1707
$8D$	0.1280	0.1632

$$\theta = \frac{C_T cos^2\gamma sin\gamma}{2(1+2k_w x/D)} \tag{C1}$$

Here γ is the yaw angle and k_w is the wake expansion factor. However, this model over predicts wake deflection due to the top-hat assumption not being accurate [40]. A new formula was proposed by Bastankhah and Porté-Agel [23] using a Gaussian distribution for the velocity deficit.

$$\begin{aligned}\frac{y_d}{D} =& \theta_0\frac{x_0}{D} + \frac{\theta_0}{14.7}\sqrt{\frac{cos\gamma}{k_y k_z C_T}}(2.9+1.3\sqrt{1-C_T}-C_T) \\ &\times \ln\left(\frac{(1.6+\sqrt{C_T})(1.6\sqrt{\frac{8\sigma_y\sigma_z}{D^2 cos\gamma}})-\sqrt{C_T}}{(1.6-\sqrt{C_T})(1.6\sqrt{\frac{8\sigma_y\sigma_z}{D^2 cos\gamma}})+\sqrt{C_T}}\right)\end{aligned} \tag{C2}$$

Where y_d is the deflection normalized by the turbine diameter D. Equations for initial skew angle θ_0, potential core length x_0 and wake width $\sigma_{y,z}$ can be found in Qian and Ishihara [24]. To better specify equations for k_y and k_z, Qian and Ishihara [24] proposed a new model, equation C3. It is also based on a Gaussian velocity deficit profile together with momentum conservation in the lateral direction.

$$\begin{aligned}\frac{y_d}{D} &= \frac{y_{d0}}{D} + \frac{\sqrt{C_T cos\gamma}sin\gamma}{18.24k^*} \\ &\ln\left|\frac{\left(\frac{\sigma_0}{D}+0.24\sqrt{C_T cos^3\gamma}\right)\left(\frac{\sigma}{D}-0.24\sqrt{C_T cos^3\gamma}\right)}{\left(\frac{\sigma_0}{D}-0.24\sqrt{C_T cos^3\gamma}\right)\left(\frac{\sigma}{D}+0.24\sqrt{C_T cos^3\gamma}\right)}\right|\end{aligned} \tag{C3}$$

A final wake deflection model has been developed by Shapiro et al. [25] based on Prandtl's lifting line theory, classical momentum theory and Bernoulli's equation. This gives the wake deflection downstream of the yawed turbine δv as a function of the free stream velocity along the axis orthogonal to the yawed turbine, denoted by x'.

$$y_d(x) = \int_{-\infty}^{x}\frac{-\delta v(x')}{U_\infty}dx' \tag{C4}$$

The transverse velocity is then defined in the following manner

$$\delta v(x) = \frac{\delta v_0}{2d_w^2(x)}\left[1+erf\left(\frac{x}{\sqrt{2}\Delta_w}\right)\right] \tag{C5}$$

where δv_0 is the transverse velocity magnitude, $d_w(x)$ is the effective diameter of the wake normalized by the turbine diameter, defined as $d_w(x) = 1 + k_w ln(1+\exp[(x-2\Delta_w)/R])$, erf is an error function, and Δ_w is a characteristic width, usually set equal R. These equations are completed of with the following expression for δv_0.

$$\delta v_0 = \frac{1}{4}C_T U_\infty \cos^2\gamma\sin\gamma \tag{C6}$$

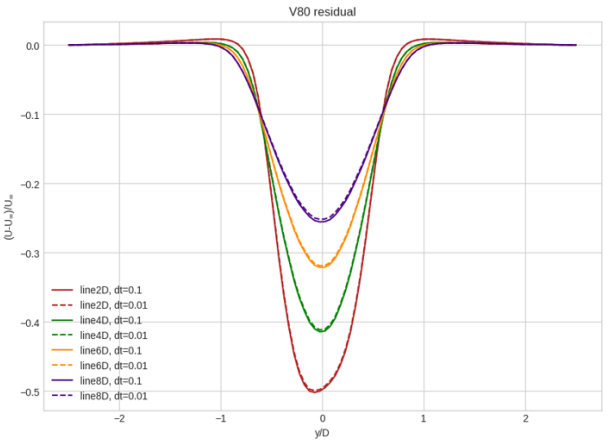

(*a*)

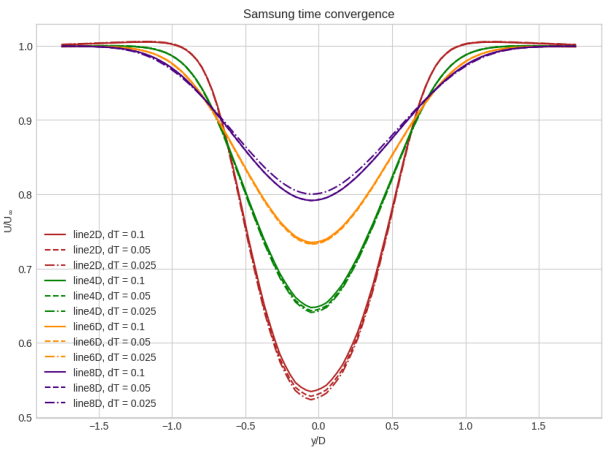

(*b*)

Fig. 21 Plot of velocity at hub height at different downstream locations for two different time steps, *(a)* being V80 and *(b)* is Samsung

Selected results for wake deflection of a 5MW NREL turbine produced in a RANS simulation during the project assignment by Fevang-Gunn and Alvestad [26] are shown in figure 25 together with the analytical wake deflection models. The model from Jimenez overpredicts wake deflection, while the others follow the wake trajectory much closer, with what could be described as a constant offset between the predicted trajectories.

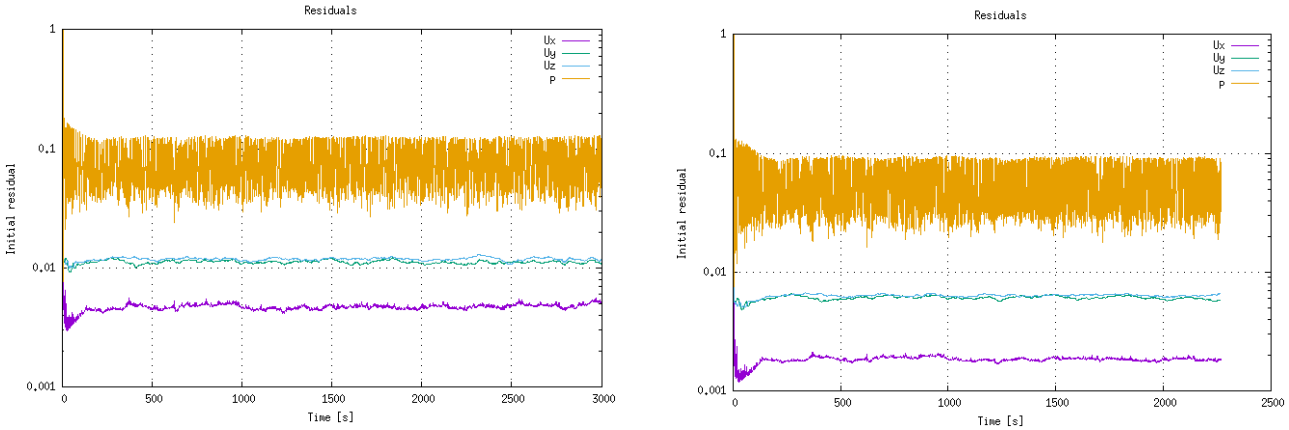

Fig. 22 Residuals for the LES reference case *(a)* and reduced time step case *(b)*. $dt = 0.1$ and $dt = 0.05$ respectively.

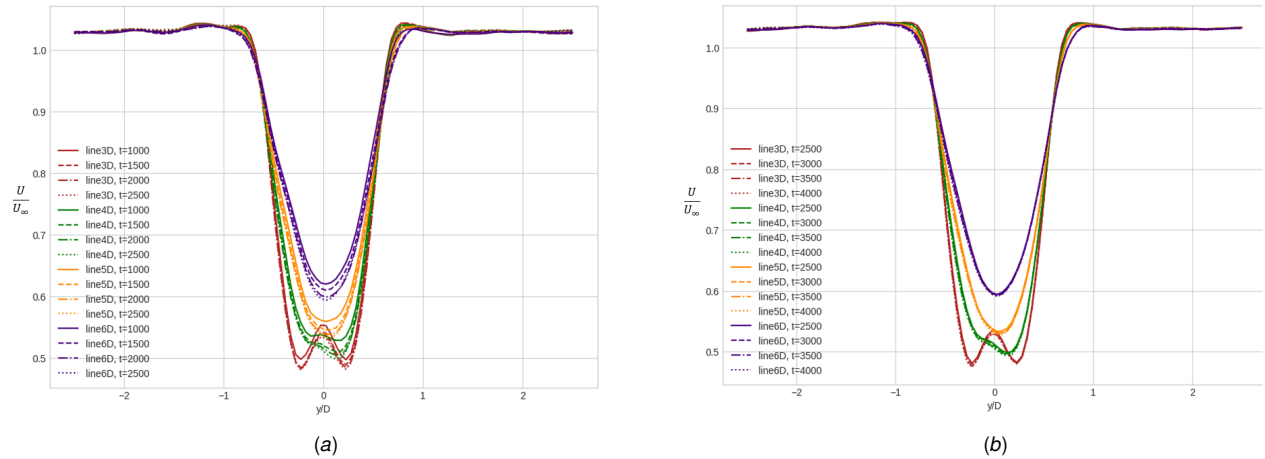

Fig. 23 Plot of velocity at hub height for different downstream locations and run-times, LES.

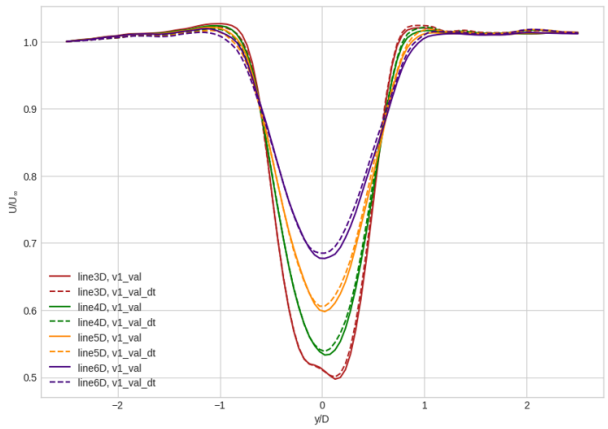

Fig. 24 Plot of velocity at hub height at different downstream locations for two different time steps, LES.

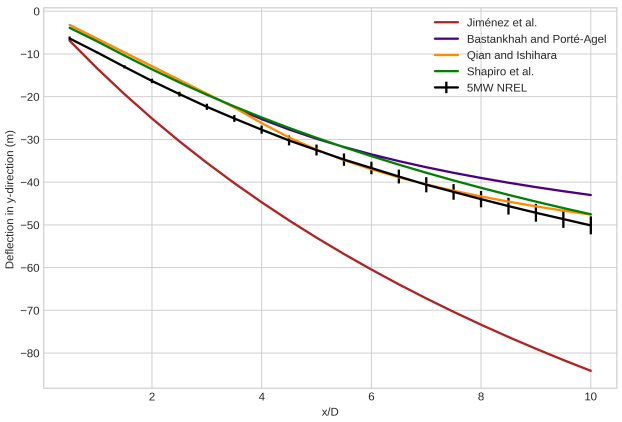

Fig. 25 Wake deflection of the 5MW NREL turbine produced by analytical models and numerical solution at 20° yaw (from [26]).

References

[1] IAE, I., 2021, "Renewables 2021: Analysis and Forecasts to 2026," .

[2] Porté-Agel, F., Bastankhah, M., and Shamsoddin, S., 2020, "Wind-Turbine and Wind-Farm Flows: A Review," Boundary-layer meteorology, **174**, pp. 1–59.

[3] Baker, R. W. and Walker, S. N., 1984, "Wake Measurements Behind a Large Horizontal Axis Wind Turbine Generator," Solar Energy, **33**(1), pp. 5–12.

[4] Ainslie, J. F., 1988, "Calculating the Flowfield in the Wake of Wind Turbines," Journal of wind engineering and Industrial Aerodynamics, **27**(1-3), pp. 213–224.

[5] Magnusson, M. and Smedman, A.-S., 1994, "Influence of Atmospheric Stability on Wind Turbine Wakes," Wind Engineering, pp. 139–152.

[6] Hancock, P. E. and Pascheke, F., 2014, "Wind-Tunnel Simulation of the Wake of a Large Wind Turbine in a Stable Boundary Layer: Part 2, the Wake Flow," Boundary-layer meteorology, **151**, pp. 23–37.

[7] Keck, R.-E., de Maré, M., Churchfield, M. J., Lee, S., Larsen, G., and Aagaard Madsen, H., 2014, "On Atmospheric Stability in the Dynamic Wake Meandering Model," Wind Energy, **17**(11), pp. 1689–1710.

[8] Aitken, M. L., Banta, R. M., Pichugina, Y. L., and Lundquist, J. K., 2014, "Quantifying Wind Turbine Wake Characteristics From Scanning Remote Sensor Data," Journal of Atmospheric and Oceanic Technology, **31**(4), pp. 765–787.

[9] Abkar, M. and Porté-Agel, F., 2015, "Influence of Atmospheric Stability on Wind-Turbine Wakes: A Large-Eddy Simulation Study," Physics of fluids, **27**(3), p. 035104.

[10] Machefaux, E., Larsen, G. C., Koblitz, T., Troldborg, N., Kelly, M. C., Chougule, A., Hansen, K. S., and Rodrigo, J. S., 2016, "An Experimental and Numerical Study of the Atmospheric Stability Impact on Wind Turbine Wakes," Wind Energy, **19**(10), pp. 1785–1805.

[11] Bingöl, F., Mann, J., and Larsen, G. C., 2010, "Light Detection and Ranging Measurements of Wake Dynamics Part I: One-Dimensional Scanning," Wind Energy: An International Journal for Progress and Applications in Wind Power Conversion Technology, **13**(1), pp. 51–61.

[12] Medici, D. and Alfredsson, P. H., 2008, "Measurements Behind Model Wind Turbines: Further Evidence of Wake Meandering," Wind Energy: An International Journal for Progress and Applications in Wind Power Conversion Technology, **11**(2), pp. 211–217.

[13] Trivellato, F. and Raciti Castelli, M., 2015, "Appraisal of Strouhal Number in Wind Turbine Engineering," Renewable and Sustainable Energy Reviews, **49**, pp. 795–804.

[14] Bastankhah, M. and Porté-Agel, F., 2019, "Wind Farm Power Optimization via Waw Angle Control: A Wind Tunnel Study," Journal of Renewable and Sustainable Energy, **11**(2), p. 023301.

[15] Fleming, P., King, J., Simley, E., Roadman, J., Scholbrock, A., Murphy, P., Lundquist, J. K., Moriarty, P., Fleming, K., van Dam, J., et al., 2020, "Continued Results From a Field Campaign of Wake Steering Applied at a Commercial Wind Farm–Part 2," Wind Energy Science, **5**(3), pp. 945–958.

[16] Churchfield, M., Wang, Q., Scholbrock, A., Herges, T., Mikkelsen, T., and Sjöholm, M., 2016, "Using High-Fidelity Computational Fluid Dynamics to Help Design a Wind Turbine Wake Measurement Experiment," *Journal of Physics: Conference Series*, Vol. 753, IOP Publishing, Paper No. 3, p. 032009.

[17] Vollmer, L., Steinfeld, G., Heinemann, D., and Kühn, M., 2016, "Estimating the Wake Deflection Downstream of a Wind Turbine in Different Atmospheric Stabilities: an LES Study," Wind Energy Science, **1**(2), pp. 129–141.

[18] Vollmer, L., 2018, "Influence of Atmospheric Stability on Wind Farm Control," Ph.D. thesis, Universität OLdenburg.

[19] Fleming, P., King, J., Dykes, K., Simley, E., Roadman, J., Scholbrock, A., Murphy, P., Lundquist, J. K., Moriarty, P., Fleming, K., et al., 2019, "Initial Results From a Field Campaign of Wake Steering Applied at a Commercial Wind Farm–Part 1," Wind Energy Science, **4**(2), pp. 273–285.

[20] Wei, D. and Wan, D., 2020, "Numerical Study of Yawed Wind Turbine Under Unstable Atmospheric Boundary Layer Flows," *International Conference on Offshore Mechanics and Arctic Engineering*, Vol. 84416, American Society of Mechanical Engineers, p. V009T09A042.

[21] Wei, D., Wang, N., Wan, D., and Strijhak, S., 2023, "Parametric Study of the Effectiveness of Active Yaw Control Based on Large Eddy Simulation," Ocean Engineering, **271**, p. 113751.

[22] Jiménez, Á., Crespo, A., and Migoya, E., 2010, "Application of a LES Technique to Characterize the Wake Deflection of a Wind Turbine in Yaw," Wind energy, **13**(6), pp. 559–572.

[23] Bastankhah, M. and Porté-Agel, F., 2016, "Experimental and Theoretical Study of Wind Turbine Wakes in Yawed Conditions," Journal of Fluid Mechanics, **806**, pp. 506–541.

[24] Qian, G.-W. and Ishihara, T., 2018, "A New Analytical Wake Model for Yawed Wind Turbines," Energies, **11**(3), p. 665.

[25] Shapiro, C. R., Gayme, D. F., and Meneveau, C., 2018, "Modelling Yawed Wind Turbine Wakes: A Lifting Line Approach," Journal of Fluid Mechanics, **841**, p. R1.

[26] Fevang-Gunn, L. and Alvestad, B. L., 2022, "Simulating the Effect of Yaw Misalignment on Wake Dynamics in the Uniform Flow Using High Fidelity Models," .

[27] Rivera-Arreba, I., Wise, A. S., Hermile, M., Chow, F. K., and Bachynski-Polić, E. E., 2022, "Effects of Atmospheric Stability on the Structural Response of a 12 MW Semisubmersible Floating Wind Turbine," Wind Energy, **25**(11), pp. 1917–1937.

[28] Bossanyi, E., Browne, I., Fraser, M., Keogh, W., Simon, E., and Skeen, N., 2022, "Validation of Controller Adaptations: Deliverable no. D3. 7," .

[29] Sørensen, J. and Shen, W., 2002, "Numerical Modelling of Wind Turbine Wakes," Journal of Fluids Engineering, **124**(2), pp. 393–399.

[30] Foti, D., Yang, X., Campagnolo, F., Maniaci, D., and Sotiropoulos, F., 2018, "Wake Meandering of a Model Wind Turbine Operating in Two Different Regimes," Physical Review Fluids, **3**(5), p. 054607.

[31] Serret, J., Tezdogan, T., Stratford, T., Thies, P. R., and Venugopal, V., 2019, "Baseline Design of the Deep Turbine Installation-Floating, a New Floating Wind Concept," *International Conference on Offshore Mechanics and Arctic Engineering*, Vol. 58769, American Society of Mechanical Engineers, p. V001T01A035.

[32] Jonkman, J., Butterfield, S., Musial, W., and Scott, G., 2009, "Definition of a 5-MW Reference Wind Turbine for Offshore System Development," National Renewable Energy Lab.(NREL), Golden, CO (United States).

[33] Quon, E., 2017, "Samwich Box: Simulated and Measured Wake Identification and Characterization Toolbox¶," https://ewquon.github.io/waketracking/index.html

[34] Carbajo Fuertes, F., Markfort, C. D., and Porté-Agel, F., 2018, "Wind Turbine Wake Characterization with Nacelle-Mounted Wind Lidars for Analytical Wake Model Validation," Remote sensing, **10**(5), p. 668.

[35] Taylor, G. I., 1938, "The Spectrum of Turbulence," Proceedings of the Royal Society of London. Series A-Mathematical and Physical Sciences, **164**(919), pp. 476–490.

[36] De Maré, M. and Mann, J., 2014, "Validation of the Mann Spectral Tensor for Offshore Wind Conditions at Different Atmospheric Stabilities," *Journal of Physics: Conference Series*, Vol. 524, IOP Publishing, Paper No. 1, p. 012106.

[37] Nybø, A., Nielsen, F. G., Reuder, J., Churchfield, M. J., and Godvik, M., 2020, "Evaluation of Different Wind Fields for the Investigation of the Dynamic Response of Offshore Wind Turbines," Wind Energy, **23**(9), pp. 1810–1830.

[38] Panjwani, B., Popescu, M., Samseth, J., Meese, E., and Mahmoudi, J., 2014, "OffWindSolver: Wind Farm Design Tool Based on Actuator Line/Actuator Disk Concept in OpenFoam Architecture," *ITM Web of Conferences*, Vol. 2, EDP Sciences, p. 04001.

[39] Pope, S. B. and Pope, S. B., 2000, *Turbulent Flows*, Cambridge university press.

[40] Ishihara, T., Yamaguchi, A., and Fujino, Y., 2004, "Development of a New Wake Model Based on a Wind Tunnel Experiment," Global wind power, **6**.

[41] Stull, R. B., 1988, *An Introduction to Boundary Layer Meteorology*, Vol. 13, Springer Science & Business Media.

[42] Jacobson, M. Z., 1999, *Fundamentals of Atmospheric Modeling*, Cambridge university press.

[43] 1990, "Evaluation of Stability Corrections in Wind Speed Profiles Over the North Sea," Journal of Wind Engineering and Industrial Aerodynamics, **33**(3), pp. 551–566.

[44] Serret, J., Rodriguez, C., Tezdogan, T., Stratford, T., and Thies, P., 2018, "Code Comparison of a NREL-Fast Model of the Levenmouth Wind Turbine with the GH Bladed Commissioning Results," *International conference on offshore mechanics and arctic engineering*, Vol. 51319, American Society of Mechanical Engineers, p. V010T09A054.

[45] Rivera-Arreba, I., Wise, A. S., Eliassen, L. V., and Bachynski-Polić, E. E., 2023, "Effect of Atmospheric Stability on the DWM Applied to Two 12 MW Floating Wind Turbines," Under review.

[46] Davidson, P., 2015, *Turbulence: An Introduction for Scientists and Engineers*, Oxford University Press.

[47] Celik, I. B., Ghia, U., Roache, P. J., and Freitas, C. J., 2008, "Procedure for Estimation and Reporting of Uncertainty Due to Discretization in CFD Applications," Journal of fluids Engineering-Transactions of the ASME, **130**(7).

[48] Gebraad, P. M., Teeuwisse, F. W., Van Wingerden, J., Fleming, P. A., Ruben, S. D., Marden, J. R., and Pao, L. Y., 2016, "Wind Plant Power Optimization Through Yaw Control Using a Parametric Model for Wake Effects — A CFD Simulation Study," Wind Energy, **19**(1), pp. 95–114.

[49] Ishihara, T., Yamaguchi, A., and Fujino, Y., 2004, "Development of a New Wake Model Based on a Wind Tunnel Experiment," Global wind power, **6**.

[50] Alfonsi, G., 2009, "Reynolds-Averaged Navier-Stokes Equations for Turbulence Modeling," Applied Mechanics Reviews - APPL MECH REV, **62**.

[51] Brugger, P., Markfort, C., and Porté-Agel, F., 2022, "Field Measurements of Wake Meandering at a Utility-Scale Wind Turbine with Nacelle-Mounted Doppler Lidars," Wind Energy Science, **7**(1), pp. 185–199.

[52] Foti, D., Yang, X., and Sotiropoulos, F., 2018, "Similarity of Wake Meandering for Different Wind Turbine Designs for Different Scales," Journal of Fluid Mechanics, **842**, pp. 5–25.

[53] Peña, A., Réthoré, P.-E., and van der Laan, M. P., 2016, "On the Application of the Jensen Wake Model Using a Turbulence-Dependent Wake Decay Coefficient: the Sexbierum Case," Wind Energy, **19**(4), pp. 763–776.

[54] Qian, G.-W. and Ishihara, T., 2017, "A Numerical Study of Wind Turbine Wake by Large Eddy Simulation and Proposal for a New Analytical Wake Model," London UK.

NTNU

Norwegian University of
Science and Technology